The Atmospheric Bridge: The Influence of ENSO Teleconnections on Air–Sea Interaction over the Global Oceans

MICHAEL A. ALEXANDER

NOAA–CIRES Climate Diagnostics Center, Boulder, Colorado

ILEANA BLADÉ

Laboratori d'Enginyeria Maritima, Universitat Politècnica de Catalunya, Barcelona, Spain

MATTHEW NEWMAN

NOAA–CIRES Climate Diagnostics Center, Boulder, Colorado

JOHN R. LANZANTE AND NGAR-CHEUNG LAU

NOAA/Geophysical Fluid Dynamics Laboratory, Princeton, New Jersey

JAMES D. SCOTT

NOAA–CIRES Climate Diagnostics Center, Boulder, Colorado

(Manuscript received 31 July 2001, in final form 1 March 2002)

ABSTRACT

During El Niño–Southern Oscillation (ENSO) events, the atmospheric response to sea surface temperature (SST) anomalies in the equatorial Pacific influences ocean conditions over the remainder of the globe. This connection between ocean basins via the ''atmospheric bridge'' is reviewed through an examination of previous work augmented by analyses of 50 years of data from the National Centers for Environmental Prediction–National Center for Atmospheric Research (NCEP–NCAR) reanalysis project and coupled atmospheric general circulation (AGCM)–mixed layer ocean model experiments. Observational and modeling studies have now established a clear link between SST anomalies in the equatorial Pacific with those in the North Pacific, north tropical Atlantic, and Indian Oceans in boreal winter and spring. ENSO-related SST anomalies also appear to be robust in the western North Pacific during summer and in the Indian Ocean during fall. While surface heat fluxes are the key component of the atmospheric bridge driving SST anomalies, Ekman transport also creates SST anomalies in the central North Pacific although the full extent of its impact requires further study. The atmospheric bridge not only influences SSTs on interannual timescales but also affects mixed layer depth (MLD), salinity, the seasonal evolution of upper-ocean temperatures, and North Pacific SST variability at lower frequencies. The model results indicate that a significant fraction of the dominant pattern of low-frequency (>10 yr) SST variability in the North Pacific is associated with tropical forcing. AGCM experiments suggest that the oceanic feedback on the extratropical response to ENSO is complex, but of modest amplitude. Atmosphere–ocean coupling outside of the tropical Pacific slightly modifies the atmospheric circulation anomalies in the Pacific–North America (PNA) region but these modifications appear to depend on the seasonal cycle and air–sea interactions both within and beyond the North Pacific Ocean.

1. Introduction

While air–sea interactions responsible for El Niño and the Southern Oscillation (ENSO) are centered in the equatorial Pacific Ocean, changes in tropical convection associated with ENSO influence the global atmospheric circulation. The ENSO-driven large-scale atmospheric teleconnections alter the near-surface air temperature, humidity, and wind, as well as the distribution of clouds far from the equatorial Pacific. The resulting variations in the surface heat, momentum, and freshwater fluxes can induce changes in sea surface temperature (SST), salinity, mixed layer depth (MLD), and ocean currents. Thus, the atmosphere acts as a bridge spanning from the equatorial Pacific to the North Pacific, illustrated in Fig. 1, and to the South Pacific, the Atlantic, and Indian Oceans. The ENSO-related SST anomalies that develop over the world's oceans can also feed back on the original atmospheric response to ENSO.

Corresponding author address: Michael Alexander, NOAA–CIRES Climate Diagnostics Center, R/CDC1, 325 Broadway, Boulder, CO 80305-3328.
E-mail: maa@cdc.noaa.gov

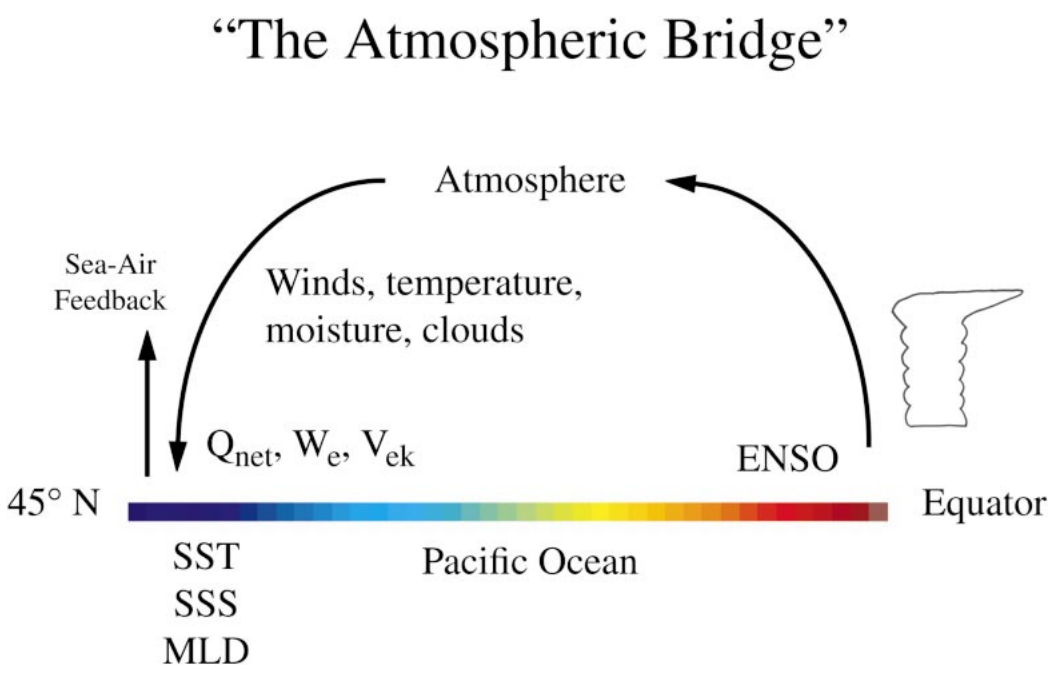

FIG. 1. Schematic of the ''atmospheric bridge'' between the tropical and North Pacific Oceans. The bridge concept also applies to the Atlantic, Indian, and South Pacific Oceans. The bridge occurs through changes in the Hadley and Walker cells, Rossby waves, and interactions between the quasi-stationary flow and storm tracks (see Trenberth et al. 1998). The Q_{net} is the net surface heat flux; w_e the entrainment rate into the mixed layer from below, which is primarily driven by surface fluxes; SST the sea surface temperature; SSS the sea surface salinity; and MLD the mixed layer depth.

The ''atmospheric bridge,'' taken here to be the tropical Pacific Ocean→atmosphere↔remote ocean connection during ENSO, warrants study because it (i) is essential for prediction of SSTs in the tropical Atlantic (Penland and Matrosova 1998) and possibly in other ocean basins as well; (ii) contributes to the leading patterns of SST variability on interannual and longer timescales in the North Pacific (Graham et al. 1994; Zhang et al. 1997; Gu and Philander 1997) and in the Indian Ocean–Asian monsoon region (Lau and Nath 2000); (iii) provides a rigorous test of our ability to simulate the global atmospheric response to ENSO, especially the temporal evolution of surface fluxes; (iv) allows for model experiments that can cleanly separate between atmospheric forcing—in this case the remote response to ENSO—and oceanic feedback on the atmosphere (e.g., Alexander 1992b); and (v) strongly influences marine ecosystems outside the equatorial Pacific (Mysak 1986; Dayton and Tegner 1990).

Beginning in the mid-1970s, researchers related observed SST anomalies in the tropical Pacific with anomalies in other ocean basins, as summarized in Table 1. Using a wide range of techniques, the studies listed in Table 1 present convincing evidence that ENSO influences the evolution of SST anomalies outside the equatorial Pacific, especially in the North Pacific, tropical Atlantic, and Indian Oceans. The global nature of the ENSO SST signal, first noted by Pan and Oort (1983, 1990), is illustrated here by Fig. 2, which shows the correlations between SST anomalies averaged over 5°N–5°S, 172°E–120°W (hereafter referred to as the ENSO index) during November–December–January (NDJ) and SST anomalies over the global oceans during the following February–March–April (FMA). We chose these periods since ENSO peaks near the end of the calendar year (Rasmusson and Carpenter 1982), while most of the ENSO-related SST anomalies outside of the tropical Pacific peak 2–6 months later (Table 1). This one-to-two season lag occurs because the atmosphere takes ~2 weeks to respond to SST anomalies in the tropical Pacific and then the ocean integrates the forcing associated with the atmospheric bridge over the next several months.

While many of the relationships between SST anomalies in the equatorial Pacific and those in other ocean basins were recognized prior to 1990, the processes responsible for the generation of the remote SST anomalies and the feedback of the SST anomalies on the atmospheric circulation were not yet clear. A major goal of the Geophysical Fluid Dynamics Laboratory (GFDL)–University Consortium, since its establishment in 1990, has been to improve our understanding of the impact of both tropical and extratropical SSTs on global climate, primarily using atmospheric general circulation model (AGCM) experiments. Through the consortium and other research efforts, our knowledge of the atmospheric bridge and its role in climate variability has advanced considerably over the past decade.

TABLE 1. Observational studies, grouped by region, that have examined the relationship between SST anomalies in the equatorial Pacific with those elsewhere over the global oceans. Also listed is the method of analyses, the period of record, months when the anomalies peak in the non-ENSO region, lag in months from when SST anomalies peak in the equatorial Pacific and the timescales of variability examined: interannual (I), decadal (D), if differentiated. The statistical methods are abbreviated: empirical orthogonal function (EOF), singular value decomposition (SVD), singular spectrum analyses (SSA), rotated principal component analyses (RPCA), canonical correlation analyses (CCA), linear inverse modeling (LIM).

Data			Time		
Study	Record	Method	Months	Lag	Scale
North Pacific					
Weare et al. (1976)	1949–73	EOFs			
Reynolds and Rassmusson (1983)	1947–80	Composites	SON		
Wright (1983)		Correlations		2–3	
Niebauer (1984, 1988)		Correlations in Bering Sea			
Wallace and Jiang (1987)	1950–79	Correlations with SO	Jul–Nov		
Hanawa et al. (1989)	1961–85	Composites, correlations	JFM		
Deser and Blackmon (1995)	1950–92	EOFs	Nov–Mar		
Zhang and Wallace (1996)	1950–94	Regression, EOFs, Rotated EOFs, SVD			
Nakamura et al. (1997)	1951–92	Prefiltered EOFs			D
Zhang et al. (1998)	1950–93	Multichannel SSA			I/D
Tropical Atlantic					
Covey and Hastenrath (1978)	1911–71	Composites			
Curtis and Hastenrath (1995)	1948–92	Composites	MAM	3–5	
Enfield and Mayer (1997)	1950–92	Correlations			
Penland and Matrosova (1998)	1950–93	LIM			
Uvo et al. (1998)	1946–85	SVD	Mar	2	
Giannini et al. (2000)	1861–1990	CCA	MAMJ	2–4	
Global Tropics					
Wolter (1987, 1989)	1948–83	Cluster analysis, RPCA			
Lanzante (1996)	1870–1988	Complex RPCA, correlations		3–6	
Toure and White (1995)	1979–91	EOFs, REOFs			
Nicholson (1997)	1948–98	Harmonic analysis, composites			
Klein et al. (1999)	1952–92	Correlation			
Global					
Pan and Oort (1983, 1990)	1958–73	Correlations		0–6	
Hsiung and Newell (1983)	1949–79	EOFS			
Yasunari (1987)	1964–81	Prefiltered composites			I
Kiladis and Diaz (1989)	1877–1988	Composites			
Nitta and Yamada (1989)	1950–87	EOFs, difference maps			I/D
Kawamura (1994)	1950–88	Rotated EOFs			
Zhang et al. (1997)	1900–93	Regressions, EOFs			I/D
Moron et al. (1998)*	1901–94	Multichannel SSA			I/D
Enfield and Mestas-Nuñez (1999)	1856–1991	Prefiltered complex EOFs			I/D
Mestas-Nuñez and Enfield (1999)	1856–1991	Prefiltered rotated EOFs			D
Garreaud and Battisti (1999)	1958–93	Regressions			I/D

* Lists additional publications that have examined observed SST relationships.

This paper is intended to serve as a review of the state of our understanding of the atmospheric bridge. In the context of our review, we will present results from new observational analyses and atmosphere–ocean model experiments, which will illustrate advances that have been made in the past and outstanding issues that remain. In particular, we will assess the influence of air–sea feedback on the original atmospheric response to ENSO in the Pacific–North American (PNA) region, which has differed among previous modeling studies (cf. Alexander 1992b; Bladé 1999; Lau and Nath 1996, 2001), and examine emerging issues such as the relationship between SST anomalies in the equatorial and North Pacific Ocean at low frequencies and the extent to which the bridge influences upper–ocean conditions besides SSTs. While a global perspective of the bridge is provided, our primary focus is on ENSO-related anomalies in the PNA region.

We briefly describe the atmosphere and ocean models and the experimental design in section 2. In section 3 we examine the global precipitation and atmospheric circulation changes resulting from the tropical SST anomalies. ENSO-related SST anomalies on interannual and decadal timescales are investigated in section 4, while section 5 examines the atmospheric bridge through the relationship between sea level pressure (SLP) and SST. In section 6, we consider how changes in the atmosphere associated with ENSO can create SST anomalies via surface energy fluxes, entrainment of subsurface waters into the surface mixed layer, and Ekman

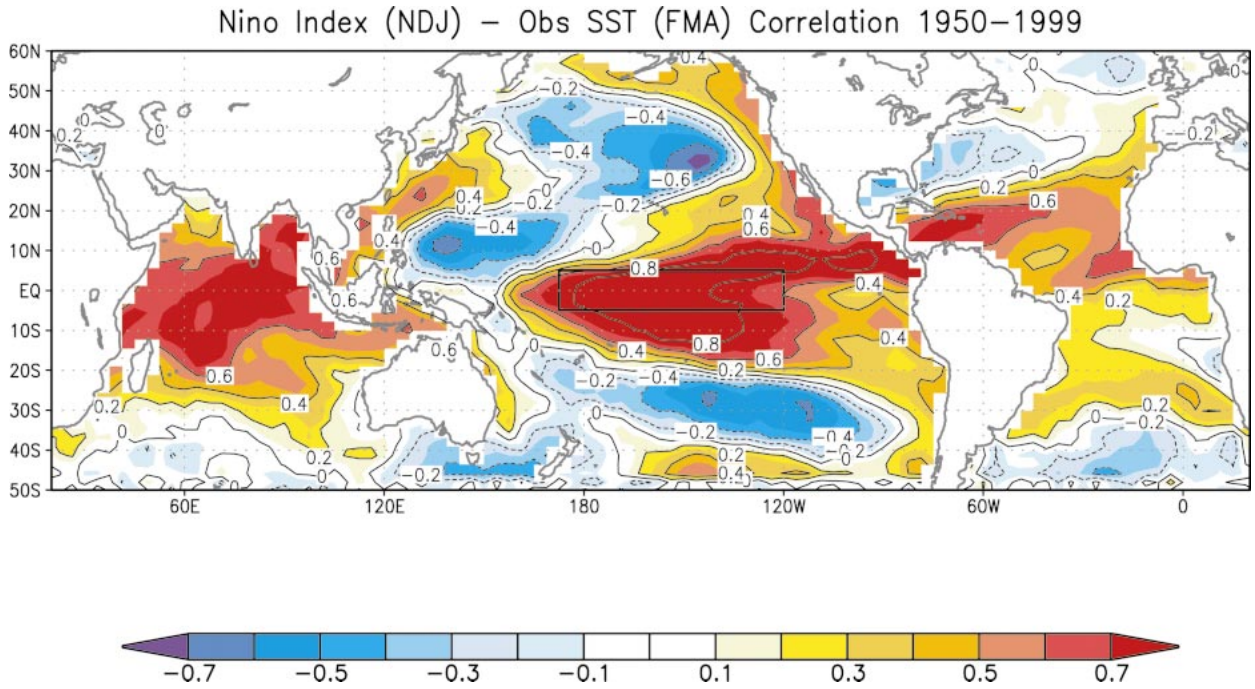

FIG. 2. Correlation between SST anomalies in the ENSO region (indicated by the box in the equatorial Pacific) in NDJ with global SST anomalies in the subsequent FMA for the period 1950–99 [shading (contour) interval is 0.1 (0.2)]. The gridded SST fields were constructed from EOFs (Smith et al. 1996) prior to 1982 and optimum interpolation of surface and satellite data (Reynolds and Smith 1994) for 1982–99.

transports. We investigate the influence of the atmospheric bridge on MLD, salinity, and the evolution of subsurface temperature anomalies in section 7. In section 8 we explore the extent to which SST anomalies generated by the atmospheric bridge feed back on the atmospheric circulation. Outstanding issues are discussed in section 9.

2. Model simulations

We have conducted three sets of AGCM experiments with different ocean configurations to examine how air–sea interaction in various ocean basins influences the atmospheric bridge. In all of the experiments, SSTs are prescribed to evolve according to observations over the period 1950–99 in the eastern tropical Pacific Ocean (15°S–15°N, 172°E–South American coast). The experiments differ in their treatment of the ocean outside of this region. In the ''control'' experiment, climatological SSTs, which repeat the same seasonal cycle each year, are specified at all remaining ocean grid points outside the tropical Pacific region. [This experiment design is often referred to as the Tropical Ocean Global Atmosphere (TOGA) in the literature.] In the mixed layer model (''MLM'') experiment, a grid of column ocean models is coupled to the atmosphere at each AGCM grid point over the ice-free ocean outside the tropical Pacific region. In the North Pacific–mixed layer model (''NP–MLM'') experiment, the ocean model is only active in the Pacific north of 21.24°N; climatological SSTs are specified elsewhere over the world oceans except in the eastern tropical Pacific. Due to the absence of ocean currents and errors in the atmosphere and ocean model, surface heat and salt flux corrections are applied to maintain the ocean model's mean seasonal cycle close to observations. Small biases in SST (<1°C), however, still occur in the long-term monthly means at a few locations after the corrections are applied. Thus, we use the long-term monthly mean SSTs from the MLM experiment to obtain the ocean boundary conditions in the control and in the NP–MLM simulations in their respective prescribed SST domains, insuring that the same SST base state is used in the three experiments. In all simulations sea ice is prescribed to repeat the climatological seasonal cycle and the ocean model is not active beneath the ice in either MLM experiment. The experiments consist of an ensemble of simulations where the individual members are initiated from different atmospheric states obtained from a long GFDL AGCM simulation. There are eight control, eight NP–MLM and 16 MLM simulations. In sections 3–7, we focus on the MLM experiment; the control and NP–MLM experiments will be used to diagnose the role of air–sea feedback on the atmospheric circulation in section 8.

All experiments have been performed with the GFDL R30 AGCM, which has an equivalent horizontal resolution of ~2.25° latitude by 3.75° longitude and 14 vertical sigma levels. The model was described in detail

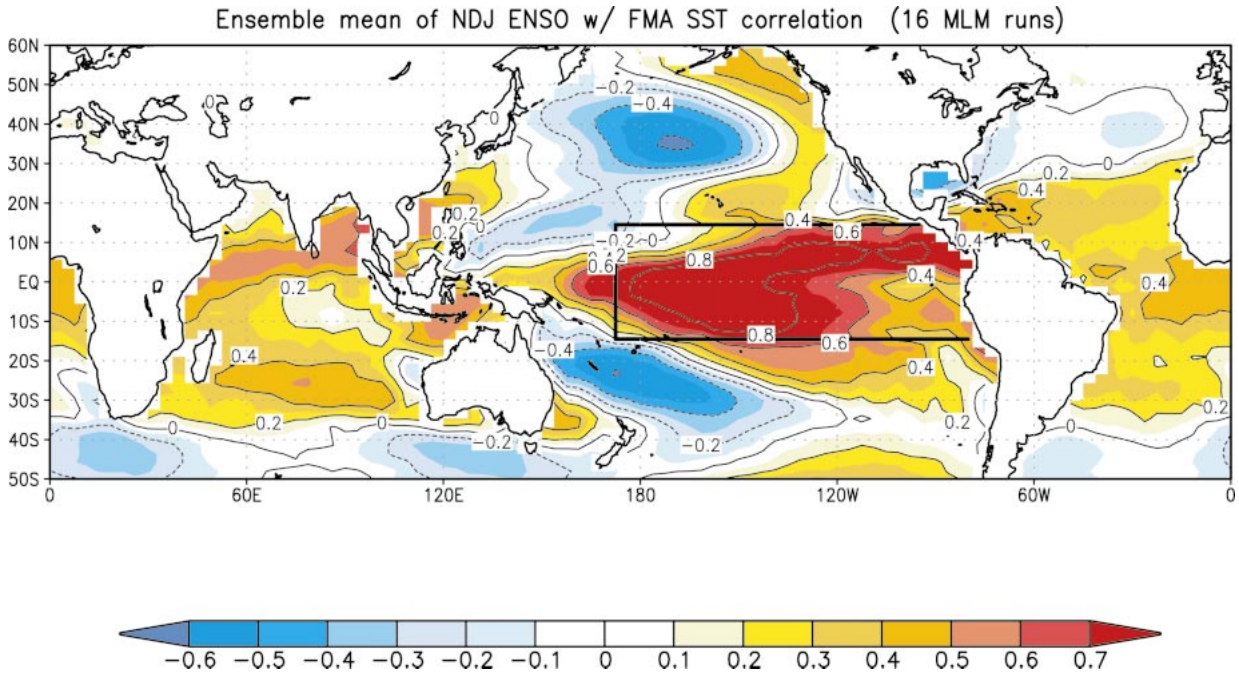

FIG. 3. As in Fig. 2 but for the ensemble average correlation in the MLM between the NDJ ENSO index and FMA global SST anomalies for the period 1950–99 [shading (contour) interval is 0.1 (0.2)]. To properly weight the ensemble members, the gridpoint correlations from the individual simulations are first transformed into Fisher's z statistics, averaged together, and then transformed back to correlation values.

by Gordon and Stern (1982) and Broccoli and Manabe (1992), while many features of the model's climate were presented in Alexander and Scott (1995) and Collins et al. (2001).

The MLM consists of a grid of independent column models that include a bulk mixed layer atop a multilayer system, where the latter represents conditions in the pycnocline. The bulk model, based on the formulation of Gaspar (1988), simulates the mixed layer temperature (equivalent to SST), salinity, and depth. The model includes local atmosphere–ocean fluxes, penetrating solar radiation, and the turbulent entrainment of water into the mixed layer, but not mean vertical motions or horizontal processes. Beneath the mixed layer, heat is redistributed via convective overturning, vertical diffusion, and penetrating solar radiation. The bottom of each column is 1000 m or the actual depth of the ocean, whichever is shallower. For open-ocean points there are 31 levels from the surface to 1000 m with 15 layers in the upper 100 m. All layers completely within the mixed layer are set to the bulk model values. The ocean model and the method used to couple it to the R30 AGCM, including the flux correction, were described in more detail in Alexander et al. (2000).

The fidelity of the model's simulation of the atmospheric bridge can be assessed by comparing the map of the ENSO index–global SST correlations averaged over the 16 MLM simulations (Fig. 3) with its observed counterpart (Fig. 2). The model reproduces the large-scale signature of the atmospheric bridge but with some differences with observations in the detailed structure. Some of these differences might arise from internal atmosphere–ocean variability, as indicated by the spread among the ensemble members. The standard deviation of the ENSO–SST correlations over the 16 MLM simulations, a measure of the spread, is <0.2 all locations and <0.1 in the centers of maximum and minimum correlation located in the central North Pacific, Indian, and tropical Atlantic Oceans (not shown). The relationship between SST anomalies and ENSO, including the spread among ensemble members, is explored further in sections 5 and 6.

3. Response to ENSO: Precipitation and upper-atmospheric circulation

The atmospheric response to tropical SST anomalies, the first element of the atmospheric bridge, has been studied extensively since Bjerknes (1966, 1969) linked warm SST anomalies in the equatorial Pacific to a deeper than normal Aleutian low. Our discussion and analyses of the atmospheric response to ENSO is brief, since Lau (1997), Trenberth et al. (1998), and Hoerling and Kumar (2002, this issue) extensively reviewed this subject. Teleconnections between the tropical Pacific and remainder of the globe have been found in numerous observational analyses (e.g., Horel and Wallace 1981; Ropelewski and Halpert 1987; Wallace et al. 1998; Winkler et al. 2001) and AGCM experiments (Rowntree 1972; Blackmon et al. 1983; Ferranti et al. 1994). In AGCMs, the response to tropical SSTs (''signal'') is embedded in internal atmospheric variability (''noise''),

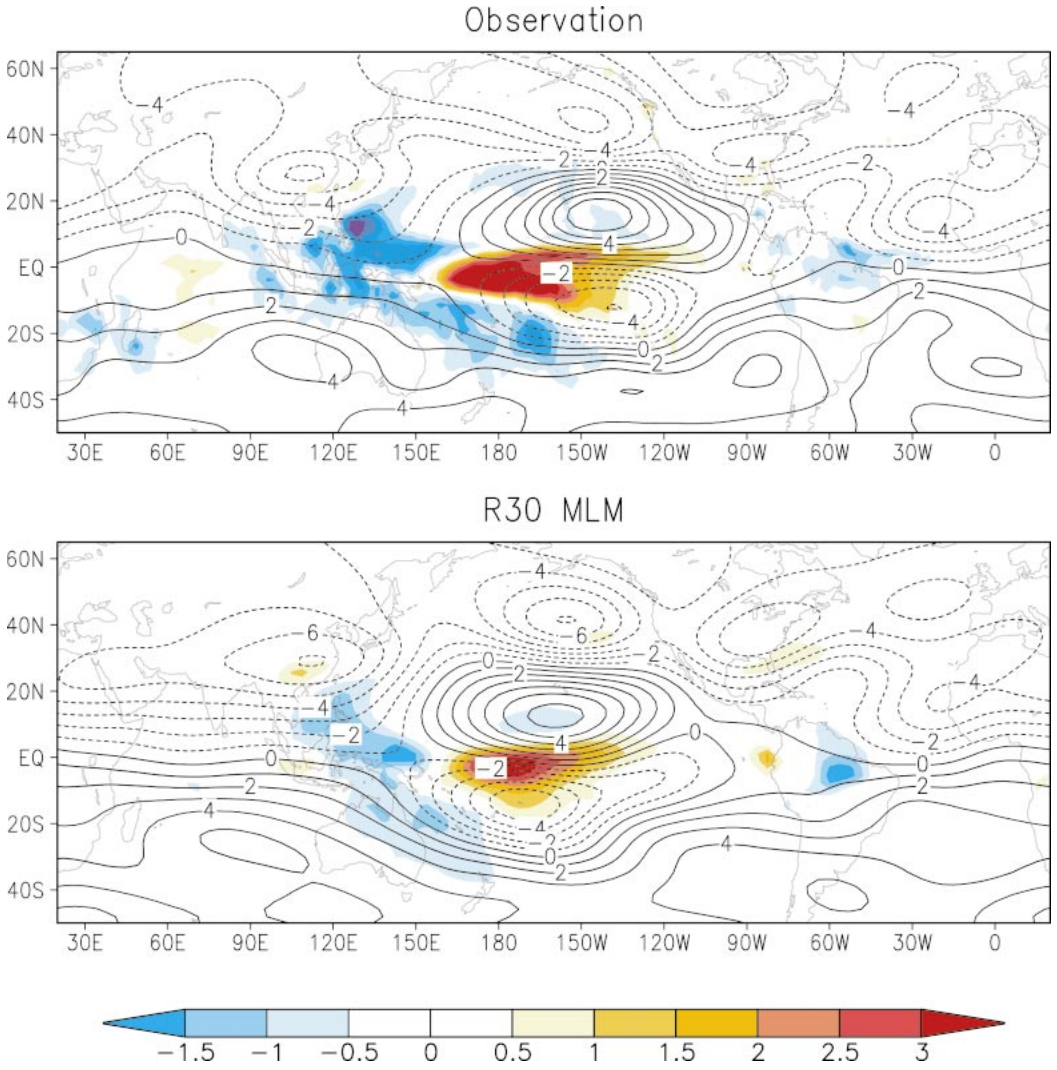

FIG. 4. Regression values of precipitation (shaded; interval is 0.5 mm day^{-1} °C^{-1}) and 200-mb streamfunction (contour; interval is 1 × 10^6 m^2 day^{-1} °C^{-1}) regressed on DJF ENSO index for DJF (1951–99) for (a) observation and (b) MLM. Changes in the nondivergent component of the upper-tropospheric circulation accompanying ENSO may be inferred from the contour lines: positive (negative) extremes are associated with anomalous clockwise (counterclockwise) flows.

requiring either long simulations or a large ensemble of simulations to obtain statistically significant results (Kumar and Hoerling 1998; Sardeshmukh et al. 2000). The dynamical link between the Tropics and extratropics involves the excitation of Rossby waves by both tropical convection (Hoskins and Karoly 1981) and the associated divergent outflow in regions of strong vorticity gradients (Sardeshmukh and Hoskins 1988). The perturbations that propagate to the extratropics are further influenced by interactions with asymmetries in the zonal mean flow (Simmons et al. 1983; Ting and Sardeshmukh 1993) and with midlatitude storm tracks (Kok and Opsteegh 1985; Held et al. 1989).

The atmospheric anomalies associated with equatorial Pacific SST anomalies are shown in Fig. 4 by regressing precipitation (color shading) and 200-mb streamfunction (contours) on the ENSO index during December–January–February (DJF). The observed fields in Fig. 4 are based on winds from the National Centers for Environmental Prediction–National Center for Atmospheric Research (NCEP–NCAR) reanalysis project (Kalnay et al. 1996; Kistler et al. 2001) and the precipitation from the Climate Prediction Center (CPC) Merged Analysis of Precipitation (CMAP) dataset (Xie and Arkin 1997), while the corresponding simulated fields are from the 16-member ensemble means of the MLM experiment.

During El Niño (warm ENSO) events, both the observed and model precipitation patterns are characterized by enhanced rainfall over the central equatorial Pacific and below-normal rainfall over Indonesia/western tropical Pacific and northern Brazil. The simulated

precipitation anomalies between 90°E and 180° are weaker and of smaller extent than in nature. A pair of anticyclones straddles the positive precipitation center over the central equatorial Pacific, similar to the atmospheric response to diabatic heating on the equator in shallow-water models (Matsuno 1966; Gill 1980). The anomalous westward flow along the equator east of the date line indicates eastward displacement of the Walker circulation during warm events. The extratropical flow is characterized by enhanced westerlies from 20° to 40° latitude in both the North and South Pacific, and by wavelike features with centers in the northeastern Pacific, Canada, eastern United States, and southern China. The MLM reproduces most of these features quite accurately, although the streamfunction anomalies over the tropical Pacific are displaced west of their observed locations. The precipitation and circulation anomalies from the GFDL R15 (~4.45° latitude × 7.5° longitude) AGCM, the model used in many previous consortium studies, were substantially weaker than the R30 estimates.

4. ENSO-related SST anomalies

Along with enhanced comprehension of atmospheric ENSO teleconnections, another key development in the atmospheric bridge hypothesis was identifying relationships between SST anomalies in various parts of the global ocean and those in the equatorial Pacific. Previous research focused on SST anomalies in the North Pacific, tropical North Atlantic, and Indian Oceans, where the ENSO signal is strong (Table 1, Fig. 2).

a. North Pacific

The relationship between SST anomalies in the tropical and North Pacific was first revealed by Weare et al. (1976) through EOF analyses of SST anomalies in all calendar months. This study, as well as more recent EOF analyses (e.g., Deser and Blackmon 1995; Zhang and Wallace 1996), found that the dominant pattern of Pacific SST variability has anomalies of one sign in the equatorial Pacific and along the coast of North America and anomalies of the opposite sign extending from ~140°W to the coast of Asia between about 25° and 50°N. The corresponding principal component [(PC), which shows the amplitude and polarity of the pattern over time] indicates that during El Niño events anomalously warm (cold) water occurs in the eastern (central) North Pacific and vice versa during La Niña events. Other observational analyses confirmed the EOF results and established that ENSO-related SST anomalies occur in the Bering Sea (Niebauer 1984, 1988) and South China Sea (Hanawa et al. 1989) in winter and in the North Pacific during summer/fall (Reynolds and Rasmusson 1983; Wallace and Jiang 1987). The former also appear in Figs. 2 and 3, while the evolution of the SST anomalies over the seasonal cycle is discussed further in section 5.

Several recent observational studies have examined the patterns of SST anomalies in the Pacific as a function of timescale (Table 1). Zhang et al. (1997) utilized several analysis techniques to separate interannual ENSO variability from a residual containing the remaining (>~7 yr) ''interdecadal'' variability. The pattern based on low-pass filtered data north of 20°S is similar to the unfiltered pattern, except it is broader in scale in the eastern equatorial Pacific and has enhanced weighting in the North Pacific relative to the Tropics. Using multichannel singular spectrum analyses, Zhang et al. (1998) found that variability on quasi-quadrennial (50–60 months) and interdecadal timescales has strong signatures in both the tropical and North Pacific. While these studies suggest that decadal variability in the North Pacific may result from the low-frequency component of ENSO, others (e.g., Latif and Barnett 1994, 1996; Pierce et al. 2000) have indicated that the variability with a period of roughly 20–30 yr, termed the Pacific Decadal Oscillation (PDO) by Mantua et al. (1997), is inherent to the extratropics.

To what extent does the atmospheric bridge contribute to decadal variability over the North Pacific, including the PDO? We address this question by comparing the observed and simulated dominant pattern and associated time series of wintertime decadal SST variability over the North Pacific (Fig. 5). The spatial patterns, obtained from EOF analyses, are based on the monthly SST anomalies that were first low-pass filtered to retain periods greater than ~10 yr and then averaged together from November to March. The EOF obtained from the MLM was computed from the ensemble average of the 16 simulations. The observed and simulated EOF 1 both explain about half of the variance and are relatively well correlated in space and time, with a spatial (temporal) correlation of 0.71 (0.69). The temporal correlations are generally lower for the individual ensemble members: that is, the projection of the individual simulations on the observed EOF 1 (Fig. 5a) correlated with the observed PC 1 yielded a 16-member average of 0.54 with a standard deviation of 0.2. The observed and MLM PCs are well correlated with the low-pass filtered ENSO index time series, with correlations of 0.77 and 0.90, respectively. We also generated SST difference maps centered on 1976 (e.g., 1977–88 minus 1970–76 and 1977–98 minus 1951–76) at approximately the time a rapid transition occurred in the climate system (e.g., see Trenberth and Hurrell 1994; Miller et al. 1994). The difference patterns in the model and observations are similar and resemble the leading EOF, but the amplitude of the differences is approximately half as large in the MLM and none of the 16 simulations were able to reproduce the large change in PC 1 that occurred between the 1970s and 1980s (not shown). Overall, the model results suggest that a significant fraction (roughly ¼–½) of the variance of the dominant pattern of low-fre-

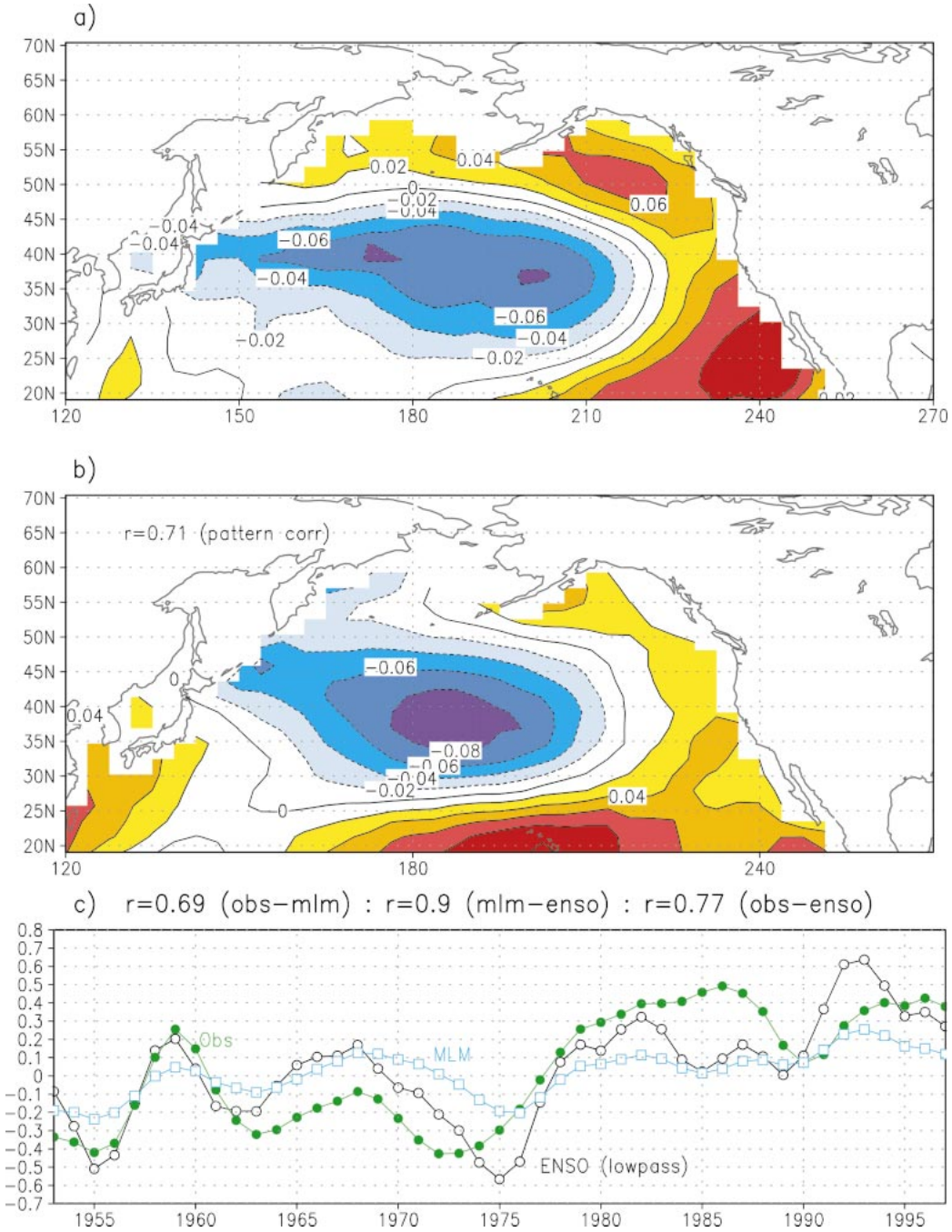

FIG. 5. EOF 1 of the low-pass filtered (>~10 yr) SST during Nov–Mar from (a) observations and (b) the MLM. (c) The first PC (time series associated with EOF 1) of the filtered SST from observations (green line), the MLM (blue line), and the ENSO index (black line). The correlations (*r*) between the three time series are given above (c).

quency SST variability in the North Pacific is associated with the atmospheric bridge.

The patterns in Fig. 5 are very similar to the dominant pattern based on unfiltered data (not shown), which Mantua et al. (1997) used to define the PDO. Processes other than the atmospheric bridge, including stochastic atmospheric forcing of the ocean and perhaps midlatitude air–sea interaction, also influence the leading pattern of North Pacific SST variability. Thus, the PDO likely includes both tropical and extratropical sources of decadal variability. Other parts of the North Pacific may be more independent from tropical influence: Deser and Blackmon (1995) and Nakamura et al. (1997) found that decadal variability in the North Pacific concentrated

along the subarctic front (~42°N, 145°E–170°W) was uncorrelated with tropical SST variability.

b. Tropical Atlantic

The link between SST anomalies in the equatorial Pacific and those in other tropical ocean basins was first examined shortly after the Weare et al. (1976) study. Using SST anomalies off the Peruvian coast as a measure of ENSO, Covey and Hastenrath (1978) constructed composites of SST, SLP, and winds in the tropical Atlantic. They found a broad region of warm SSTs to the north of the equator in boreal spring following El Niño events and roughly the opposite after La Niña events. Many subsequent observational analyses (Curtis and Hastenrath 1995; Lanzante 1996; Enfield and Mayer 1997; Klein et al. 1999; our Fig. 2) confirmed that positive SST anomalies occur in the north tropical Atlantic and Caribbean during boreal spring, approximately 3–6 months following the peak in tropical Pacific SST anomalies. Some studies (e.g., Enfield and Mayer 1997; Nicholson 1997) have found links between ENSO and SSTs in the equatorial and South Atlantic, but these relationships are weak and may not be significant.

c. Indian Ocean

Like the tropical Atlantic, the Indian Ocean warms during El Niño, with SST anomalies in that basin lagging those in the central Pacific by about 3–6 months (Lanzante 1996; Klein et al. 1999). Warming in the Indian Ocean begins earlier than in the Atlantic, starting during boreal summer/fall of the El Niño year. Over periods of 2.5–6 yr, Indian Ocean SSTs have significant variability that is coherent with Southern Oscillation fluctuations (Cadet 1985; Nicholson 1997). Additionally, the two leading patterns of SST variability in the Indian Ocean are associated with ENSO (Tourre and White 1995; Murtugudde and Busalachi 1999). For example, during the closing stage of a very strong El Niño event in 1998, SST anomalies exceeded 1°C over most of the Indian Ocean north of 20°S (Yu and Rienecker 1999). Prior to this basinwide warming, a dipole SST anomaly pattern developed along the equator during the previous fall, with positive (negative) anomalies in the western (eastern) Indian Ocean. Yu and Rienecker proposed that the dipole pattern is directly related to changes in the Walker circulation during ENSO, while Saji et al. (1999) and Webster et al. (1999) suggested that the dipole mode is independent of ENSO and is caused by local air–sea interaction.

5. SLP–SST relationships: The bridge revealed

Until the mid-1980s, studies of ENSO-related atmospheric and oceanic anomalies that formed outside of the tropical Pacific progressed on separate tracks. The two were linked by investigators who noted the close association between SST anomalies and the overlying SLP or surface wind anomalies during El Niño events.

The relationship between the Southern Oscillation index (SOI, normalized Tahiti–Darwin SLP) and global sea level pressure variations has been known since early in the twentieth century (e.g., Lockyer and Lockyer 1902; Walker 1909, 1924; Walker and Bliss 1932). Namias (1976), Trenberth and Paolino (1981), and van Loon and Madden (1981) confirmed many of the findings from the early inquiries, noting statistically significant relationships between various ENSO indices and SLP in the North Pacific during winter and spring. Simpson (1983) suggested that atmospheric teleconnections during the 1982/83 El Niño event drove changes in the California current system. Emery and Hamilton (1985) synthesized these studies with those concerning large-scale ENSO–SST relationships (e.g., Weare et al. 1976; Pan and Oort 1983) and proposed that ''the tropical Pacific Ocean may interact with the North Pacific via an atmospheric link.'' They concluded that a stronger Aleutian low during El Niño events could account for anomalously warm ocean temperatures in the northeast Pacific. As a corollary, when the North Pacific SLP anomalies differ from the canonical ENSO signal, which is not unusual (Emery and Hamilton 1985; Hanawa et al. 1989), then the corresponding SST patterns will also be different.

Two different modeling strategies were used to corroborate the atmospheric link between SST anomalies in the equatorial and North Pacific Ocean. Luksch et al. (1990) and Luksch and von Storch (1992) used an ocean GCM forced with observed surface winds and a simple atmospheric boundary layer model to estimate surface air temperature. Alexander (1990) used output from an atmospheric GCM, with and without warm SSTs specified as boundary conditions in the tropical Pacific, to drive a grid of one-dimensional mixed layer models in the North Pacific Ocean. In a follow-up experiment, Alexander (1992a) coupled the North Pacific Ocean model to the same AGCM. Both Luksch et al. and Alexander found that changes in the near-surface circulation associated with El Niño induced an SST pattern in the North Pacific that resembled observations, with cold water in the central North Pacific and warm water in the Gulf of Alaska. While these studies clearly validated the atmospheric link between the tropical and North Pacific during ENSO, Lau and Nath (1994) were the first to call this process the atmospheric bridge.

Following Rasmusson and Carpenter (1982) and Harrison and Larkin (1998), we use composite analysis to show the evolution of SLP and SST over the life cycle of ENSO events. Composites are constructed based on nine El Niño (warm) events: 1957, 1965, 1969, 1972, 1976, 1982, 1987, 1991, and 1997; and nine La Niña (cold) events: 1950, 1954, 1955, 1964, 1970, 1973, 1975, 1988, and 1998. The first eight El Niño and La Niña events were identified by Trenberth (1997), to which we added the 1997 El Niño and 1998 La Niña

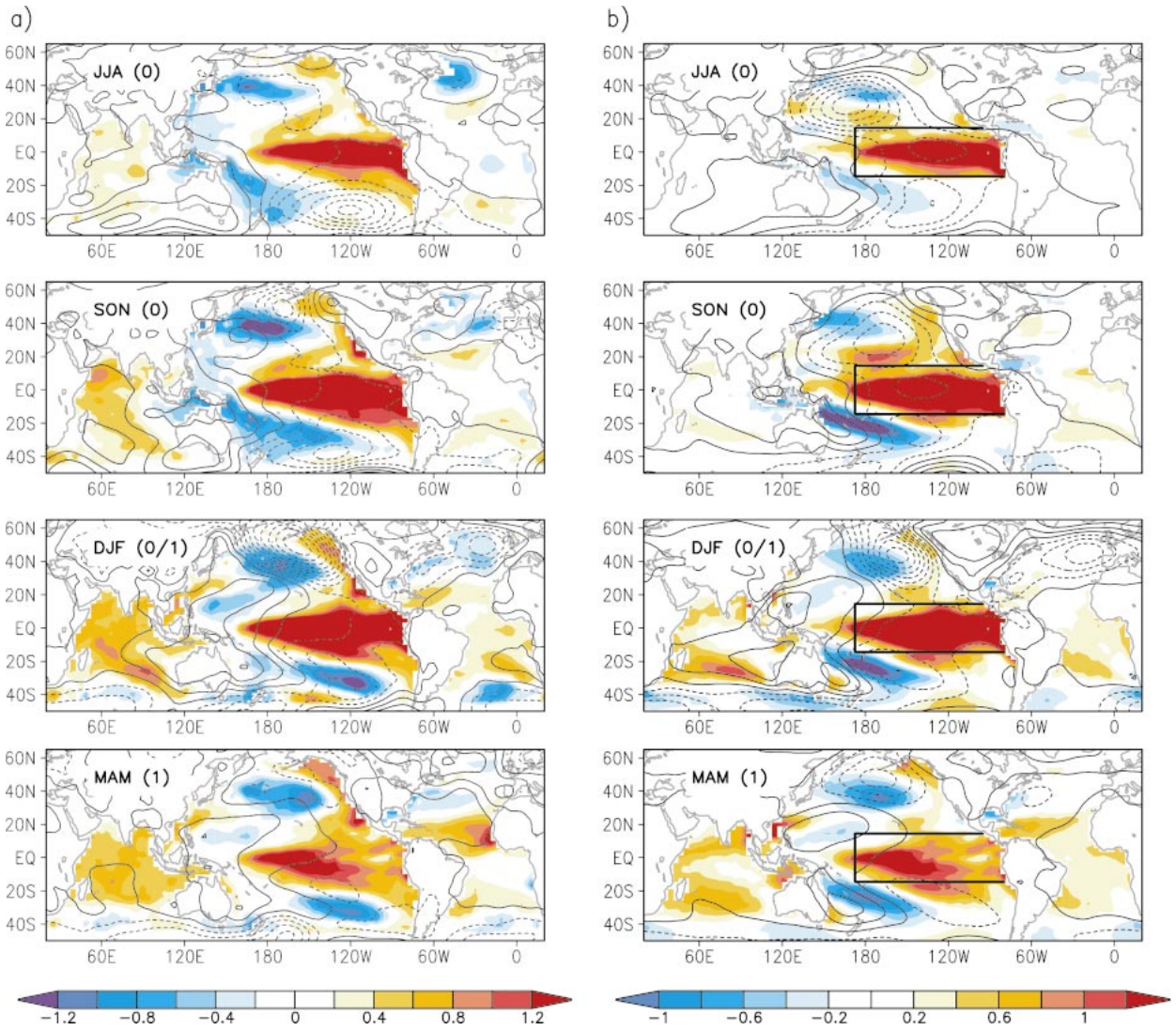

FIG. 6. (a) Observed and (b) simulated El Niño (warm) − La Niña (cold) composite of SLP (contour interval is 1 mb) and SST (shading interval is 0.2°C) for JJA(0), SON(0), DJF(0/1), and MAM(1), where 0 indicates the ENSO year and 1 the year after. The observed values are from NCEP–NCAR reanalysis and the model results from the ensemble average of the 16 MLM integrations.

events. Hereafter, the year in which ENSO peaks and the two following years are designated by (0), (1), and (2), respectively. Global maps of composite El Niño minus La Niña conditions (also referred to as warm − cold or ENSO anomalies) are presented in Fig. 6 for 3-month periods beginning in June–July–August of the ENSO year [JJA(0)] and ending in March–April–May of the following year [MAM(1)].

In nature (Fig. 6a), ENSO events are well established by JJA(0) with warm (cold) waters during El Niño (La Niña) events in the equatorial Pacific and an out-of-phase relationship between SLP in the Eastern and Western Hemisphere, characteristic of the Southern Oscillation. Cold SST anomalies have begun to form in the western part of the North and South Pacific during JJA(0) even though the anomalous circulation is quite weak. For example, one of the largest ENSO-related SST signals occurs during late summer/early fall along 40°N where the magnitude of SST anomalies exceed 1.0°C but the SLP anomalies are only ~1 mb. Large amplitude SST anomalies can form in summer since the surface fluxes are distributed over a thin mixed layer.

The observed warm − cold SLP differences in the Tropics remain relatively constant over the entire year from JJA(0) to MAM(1). During this time the warm waters that begin to form in the tropical North Atlantic during El Niño events increase in magnitude and extent, peaking in MAM(1). During JJA(0) and SON(0), SST anomalies are positive in the western Indian Ocean and negative south of Indonesia in the eastern part of the basin, consistent with the idea that the Indian Ocean SST dipole is closely tied to ENSO. As the ENSO com-

posite progresses, warm water spreads throughout the Indian Ocean and South China Sea.

In the northern extratropics, the SLP anomalies are strongest during December(0)–February(1) [DJF(0/1)] when the Aleutian low is 9 mb deeper during El Niño than in La Niña events (Fig. 6a). As a result, surface westerlies are enhanced over the central North Pacific. During El Niño, anomalous northwesterly winds advect cold air over the central North Pacific, while southerly winds advect warm moist air along the west coast of North America. The negative (positive) temperature departures in the central (eastern) North Pacific are consistent with this surface forcing.

The corresponding evolution of SLP and SST anomalies during ENSO from the ensemble average of the 16 MLM simulations is shown in Fig. 6b. The model reproduces many of the features found in the observed composite, especially in DJF(0/1)–MAM(1), which helps to confirm the essence of the atmospheric bridge hypothesis: that is, local atmospheric forcing is the primary factor in generating SST anomalies outside the tropical Pacific during ENSO. However, several discrepancies between the model and observations can be noted as well. For example, the simulated negative SLP anomalies over the North Pacific are of greater magnitude and extent than in observations in JJA(0), SON(0), and MAM(1), while the reverse is true in DJF(0/1). While some of the model–data differences could be due to internal atmospheric variability, as suggested by the spread among ensemble members (see Fig. 8), many of the differences are likely caused by model error and the absence of ocean dynamics.

6. Processes that generate SST anomalies

The atmosphere influences SST directly through surface heat fluxes and indirectly via momentum and freshwater fluxes, which subsequently affect ocean currents and turbulent mixing. Here we examine air–sea interactions in the North Pacific, tropical Atlantic, and Indian Oceans, where the atmospheric bridge has been shown to be strong.

a. North Pacific

The very strong but unanticipated 1982/83 El Niño event forced researchers to reconsider not only the fundamental dynamics of ENSO but also how ocean anomalies develop in the extratropical Pacific. Prior to the 1982/83 event, research focused on coastal Kelvin waves as the mechanism for linking tropical and extratropical SST anomalies during ENSO. These waves, however, are confined to a narrow region near the shore; for example, the internal deformation radius (*e*-folding scale) of coastal Kelvin waves is less than 50 (20) km at 20°N (45°N). While Rienecker and Mooers (1986) and Johnson and O'Brien (1990) confirmed the importance of coastally trapped waves, they, along with Simpson (1983) and Wagner (1984), showed that changes in the atmospheric circulation played a major role in altering oceanic conditions along the west coast of North America during the 1982/83 event.

In a review of El Niño, Mysak (1986) hypothesized several ways in which changes in the near-surface atmospheric circulation over the North Pacific could influence SSTs: coastal upwelling, Ekman pumping, and ocean advection—presumably through Ekman transport. Mysak and the studies mentioned above, however, did not consider surface heat fluxes. The relationship between ENSO and surface fluxes was investigated by Zhao and McBean (1986) and Cayan (1990), who correlated the SOI with air–sea heat fluxes over the North Pacific and the globe, respectively. Zhao and McBean found only a weak relationship between the SOI and surface fluxes, while Cayan found significant correlations with fluxes in the central North Pacific. The discrepancy between these two studies could result from differences in the period of record, the number and quality of the observations used in the analyses, and the coefficients used in the bulk formulas to compute the fluxes. Subsequent studies of surface fluxes (e.g., Iwasaka and Wallace 1995) have tended to confirm Cayan's analyses.

Frankignoul (1985), Qiu (2000), and Scott (2002, manuscript submitted to *J. Climate*) discussed factors that influence the evolution of extratropical SST anomalies. Here we consider the three dominant factors on interannual timescales: the net surface heat flux (Q_{net}), entrainment heat flux (Q_{we}), and Ekman transport (Q_{ek}). Alexander (1990, 1992a) showed that Q_{net} was the dominant process in generating SST anomalies in the North Pacific during ENSO, while Lau and Nath (1994, 1996, 2001) found that these SST anomalies could be fairly well simulated by a 50-m slab model forced only with surface heat fluxes. Neither study considered Q_{ek}. The anomalous Ekman heat transport, which depends primarily on the anomalous surface wind stress multiplied by the mean SST gradient, is computed here as a diagnostic, that is, it does not influence SST in the MLM.

The MLM warm − cold composites of Q_{net}, Q_{we}, and Q_{ek} during DJF (0/1) are shown in Fig. 7. Clearly, Q_{net} is the dominant factor creating SST anomalies during boreal winter, which explains why studies that use fixed-depth ocean models can simulate SST anomalies associated with ENSO reasonably well. Consistent with the low-level atmospheric circulation (Fig. 6b), the surface fluxes cool the central North Pacific and warm the Gulf of Alaska and South China Sea during El Niño. In these regions $|Q_{net}| > 40$ W m^{-2}, which leads to SST tendencies of $\sim$0.25°C month^{-1} for a typical wintertime MLD of 100 m; thus slab models where the MLD is set to 50 m overestimate the amplitude of SST anomalies in winter.

Consistent with Alexander (1990, 1992a), the maximum Q_{we} anomalies are roughly ¼–⅓ as large as those of Q_{net} (Fig. 7) but have a different pattern. During

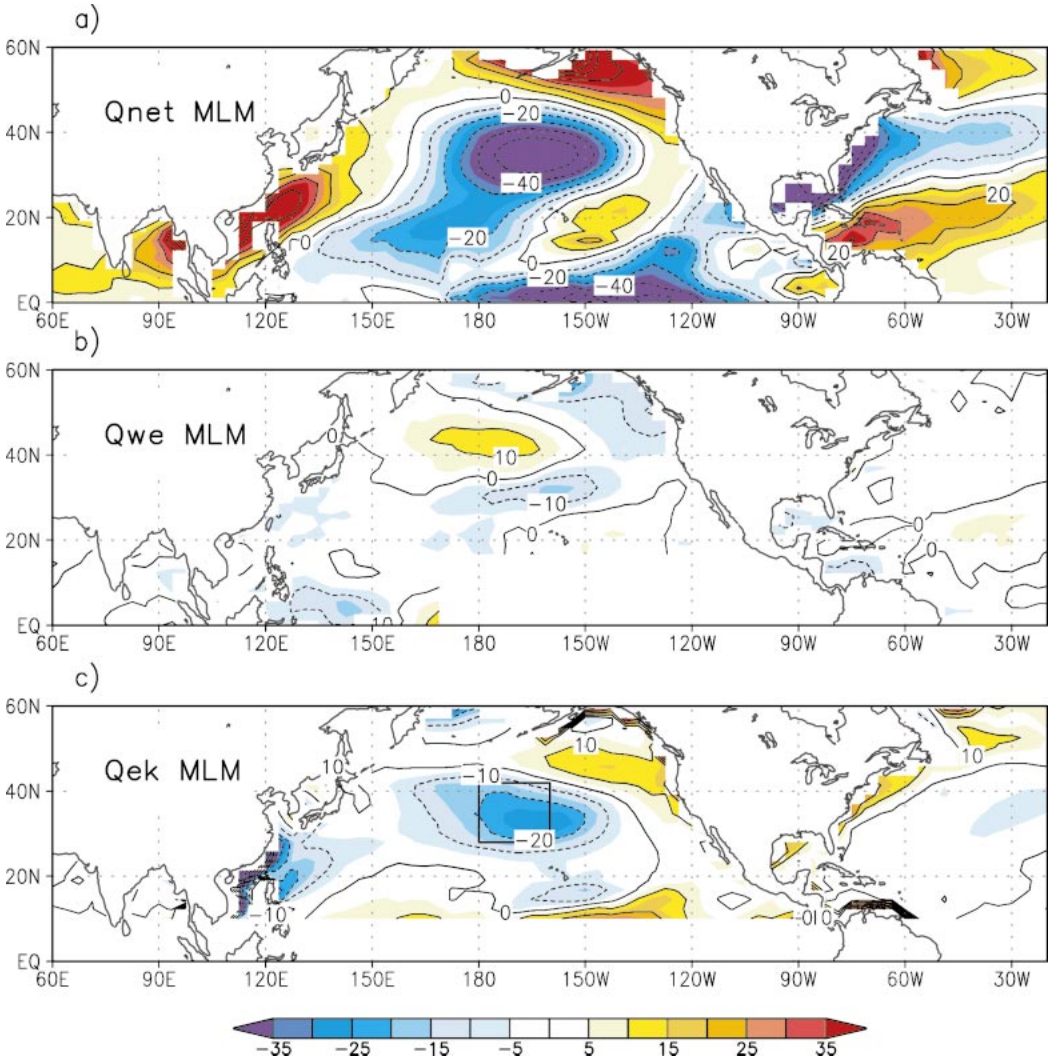

FIG. 7. The composite El Niño − La Niña (a) net heat flux to the ocean (Q_{net}), (b) entrainment heat flux (Q_{we}), (c) Ekman heat transport composites (Q_{ek}) during DJF(0/1) from the MLM. The shading (contour) interval is 5 (10) W m^{-2}. The box in (c) delineates the central North Pacific region.

winter, Q_{we} slightly enhances the cold anomaly in the central North Pacific, but primarily damps the SST anomalies over the remainder of the basin. In the ocean model, $Q_{we} = (w_e/\text{MLD})(T_{below} - \text{SST})$, where w_e is the entrainment rate and T_{below} is the temperature just below the mixed layer. Given that the time mean MLD and w_e are always positive, if the w_e and T_{below} departures from the time mean ($'$) are relatively small, then $Q'_{we} \approx -\overline{w}_e \text{SST}'/\text{MLD}$, which indicates that the anomalous heat flux at the base of the mixed layer tends to damp SST anomalies. While this is often the case (Frankignoul and Reynolds 1983), entrainment can also generate SST anomalies, depending on the season and vertical temperature structure (see section 7c).

The diagnosed Ekman heat transport is generally in phase with Q_{net} but approximately ⅓–½ as large. Enhanced westerlies in the central North Pacific during El Niño, which increase the upward surface heat flux, also cool the water through southward Ekman drift. The diagnosed MLM Q_{ek} anomalies are similar to observations but the cooling over the central North Pacific is somewhat stronger in nature (not shown).

The net surface heat flux is composed of shortwave (Q_{sw}) and longwave (Q_{lw}) radiation and sensible (Q_{sh}) and latent (Q_{lh}) heat flux. In mid- and high latitudes, sensible and latent heat fluxes dominate the generation of SST anomalies in fall and winter during ENSO (Alexander 1992a; Lau and Nath 2001). In general, Q_{lh} anomalies strongly influence SST over the entire globe, while the magnitude of the Q_{sh} (Q_{sw}) anomalies increases (decreases) when going from the Tropics toward the Poles.

The evolution of ENSO-induced SST anomalies and associated forcing terms over a region in the central

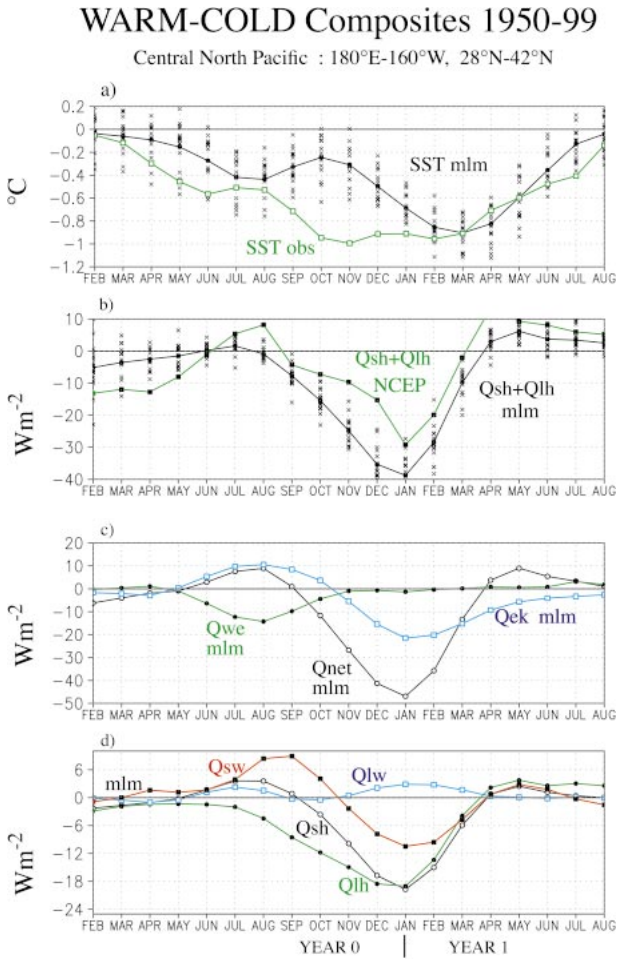

FIG. 8. Composite El Niño − La Niña time series of SST (°C) and fluxes into the mixed layer (W m^{-2}) over the ENSO cycle for a region in the central North Pacific (28°–42°N, 180°–160°W). (a) SST and (b) (Q_{lh} + Q_{sh}) heat flux from NCEP reanalysis (green), the ensemble mean MLM (solid black), and the 16 individual MLM simulations (black crosses); (c) Q_{net} (black), Q_{we} (green), Q_{ek} (blue) from the MLM; and (d) the four components of Q_{net} from the MLM: Q_{sw} (red), Q_{lw} (blue), Q_{sh} (black), and Q_{lh} (green). All curves have been smoothed using a three-month running average.

North Pacific (28°–42°N, 180°–160°W, box in Fig. 7c) is shown in Fig. 8. During fall and winter, Q_{lh} and Q_{sh}, and to a lesser extent, Q_{sw}, cool the mixed layer. While the model accurately simulates the magnitude of the SST anomalies in Feb(1)–May(1), it underestimates the cooling from Sep(0)–Jan(1), even when the spread among the 16 ensemble members is taken into account (Fig. 8a). The limited magnitude of the simulated SST anomalies in fall is somewhat surprising given that the cooling due to Q_{sh} + Q_{lh} is greater in the MLM than in the NCEP–NCAR reanalysis beginning in Aug(0) (Fig. 8b). Several factors may contribute to the underestimate of the SST anomaly in the central North Pacific: (i) errors in simulated radiative fluxes, especially Q_{sw}, (Scott and Alexander 1999); (ii) an overestimation of MLD in the MLM resulting in a reduced SST anomaly, although the simulated MLD is close to observed during fall and winter in this region; (iii) amplifying feedbacks between model errors; and (iv) processes absent from the MLM, such as Ekman transport. While the diagnosed Q_{ek} does cool the central Pacific region in late fall/early winter (Fig. 8c), other factors must contribute to the model–data differences in Sep(0)–Nov(0).

In the central North Pacific region, cooling by Q_{we} and Q_{lh} (Figs. 8c,d) is slightly larger than the warming due to Q_{sw} during the summer of Yr(0). Even though the flux anomalies are of limited magnitude they can significantly affect SSTs in summer since the mixed layer is shallow (<20 m).

b. Atlantic Ocean

During the last half of the 1990s several studies investigated the processes responsible for the warming (cooling) of the tropical North Atlantic in boreal spring following the peak of El Niño (La Niña) events. Observational analyses (Hastenrath et al. 1987; Curtis and Hastenrath 1995; Enfield and Mayer 1997; Klein et al. 1999) showed that weakening trade winds over much of the Atlantic between approximately 5° and 20°N reduced the upward latent heat flux during JFM(1). The AGCM simulations of Saravanan and Chang (2000) reproduced this finding but indicated that higher humidity associated with warmer surface air temperature also contributes to the reduced evaporation. A reduction in cloudiness (Klein et al. 1999; Lau and Nath 2001), associated with both the descending branch of the anomalous Walker circulation and with the atmospheric teleconnections that pass through the PNA sector, results in the warming of the subtropical North Atlantic in spring via enhanced Q_{sw}. ENSO may also influence SSTs in the tropical Atlantic via changes in Ekman pumping (Curtis and Hastenrath 1995) and ocean dynamics (Latif and Barnett 1995). However, Klein et al. (1999) were able to reproduce much of the observed warming associated with ENSO using only surface flux anomalies and a linear damping term. The results from the MLM simulations (Fig. 7) indicate that Q_{net} has a much larger effect on SST anomalies than Q_{we} and Q_{ek} in the subtropical North Atlantic in DJF(0/1). In the Gulf of Mexico and eastern seaboard of the United States, large Q_{net} anomalies (Fig. 7) are primarily due to anomalies in Q_{sw} and Q_{lh} (not shown).

c. Indian Ocean

Surface heat fluxes also force SST anomalies in the North Indian Ocean and South China Sea during ENSO as illustrated by Fig. 7. Cadet (1985) and Klein et al. (1999) emphasized the role of shortwave fluxes in this region, while the observational analyses of Yu and Rienecker (1999) and modeling studies by Behera et al. (2000) and Venzke et al. (2000) indicated that latent heat fluxes are the dominant term driving SST anom-

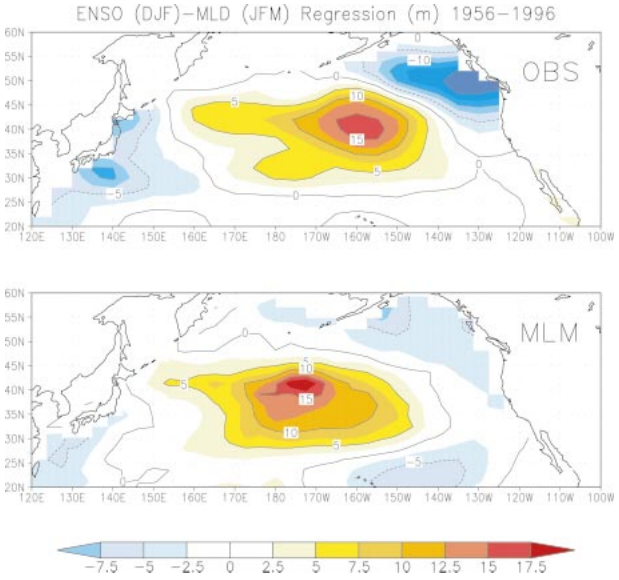

FIG. 9. MLD (m) in JFM regressed on the DJF ENSO SST derived from (a) subsurface temperature measurements from White (1995) and (b) the MLM. Both are shown for 1956–96, the period when observations are available.

alies. Ocean dynamics also appear to influence ENSO-related SST in parts of the Indian Ocean: easterly wind anomalies enhance cooling in the eastern half of the basin during SON(0) via Ekman pumping (Yu and Rienecker 1999), while Rossby waves generated by anomalous winds in the southeastern Indian Ocean may contribute to the basinwide warming in the following winter (Chambers et al. 1999). The absence of ocean dynamics may partially explain why the MLM underestimates the positive SST anomalies between 0° and 15°S in the Indian Ocean (cf. Figs. 6a and 6b).

7. Other ENSO-induced ocean changes

Most previous studies of the atmospheric bridge focused on the development of SST anomalies, yet atmospheric changes associated with ENSO also influence salinity, mixed layer depth, and the subsurface temperature structure.

a. MLD

Regressions between the DJF ENSO index and MLD anomalies in JFM over the North Pacific are shown for observations and the MLM in Fig. 9. The observed MLD provided by the Joint Environmental Data Analysis Center (JEDAC; White 1995) is defined as the depth at which the temperature is 1.0°C cooler than at the surface and is based on bathythermograph measurements for the years 1956–96, while the MLD in the MLM is computed explicitly from the turbulent kinetic energy equation. The mean MLD is well simulated in the North Pacific but is somewhat underestimated in the North Atlantic during winter (Alexander et al. 2000). The observed and simulated patterns of ENSO-related MLD anomalies are similar, although the anomaly maxima are shifted ~15° westward in the MLM, consistent with the displacement of the model's atmospheric response to tropical SST anomalies (Fig. 3). In both observations and the MLM, the mixed layer is deeper in the center of the basin and shallower in the northeast Pacific and to the south and east of Japan. Hanawa et al. (1988) also noted shoaling of the mixed layer south of Japan during El Niño events. Over the North Pacific the pattern in Fig. 9 resembles decadal changes in MLD during winter (Polovina et al. 1995; Deser et al. 1996; Miller and Schneider 2000) as well as the ENSO SST anomaly pattern (Figs. 2, 6, and 10) but with opposite polarity. The magnitude of the simulated and observed anomalies is comparable over most of the domain, although the ENSO-related shoaling of the mixed layer west of Canada is weaker in the MLM. While many factors are likely to contribute to the model–data differences in the MLD, a particularly important factor is that salinity is included in the ocean model but not in the observed MLD estimates. Salinity influences the density profile and hence the base of the mixed layer, especially north of ~45°N.

b. Salinity

ENSO can influence salinity via precipitation minus evaporation ($P - E$), river runoff, and oceanic processes. Changes in $P - E$ in the MLM result in large salinity anomalies in the Tropics, where El Niño − La Niña salinity differences exceed 0.8 parts per thousand (ppt) in the Indonesian region from Jul(0)–Apr(1) and 0.3 ppt in the Caribbean Sea from Oct(0)–Dec(0) (not shown). Schmittner et al. (2000) also found a decrease in $P - E$ to the north of South America during El Niño events in the NCEP–NCAR and European Centre for Medium-Range Weather Forecasts (ECMWF) reanalysis datasets. Schmittner et al. (2000), Latif et al. (2000), and Latif (2000) presented evidence that $P - E$ changes associated with equatorial Pacific SST anomalies impact the thermohaline circulation when the salinity anomalies in the Caribbean are advected to the sinking regions in the far North Atlantic. Lukas and Lindstrom (1991) found that salinity in the western equatorial Pacific strongly influences the density profile and thus the amount of cooling due to entrainment during westerly wind bursts. They hypothesized that regulation of SST in the warm pool region by salinity-dependent entrainment could play an important role in the ENSO cycle.

c. Reemergence of SST anomalies

The seasonal cycle of MLD has the potential to influence upper-ocean temperatures from one winter to the next. Namias and Born (1970, 1974) first noted that midlatitude SST anomalies tended to recur from one winter to the next without persisting through the inter-

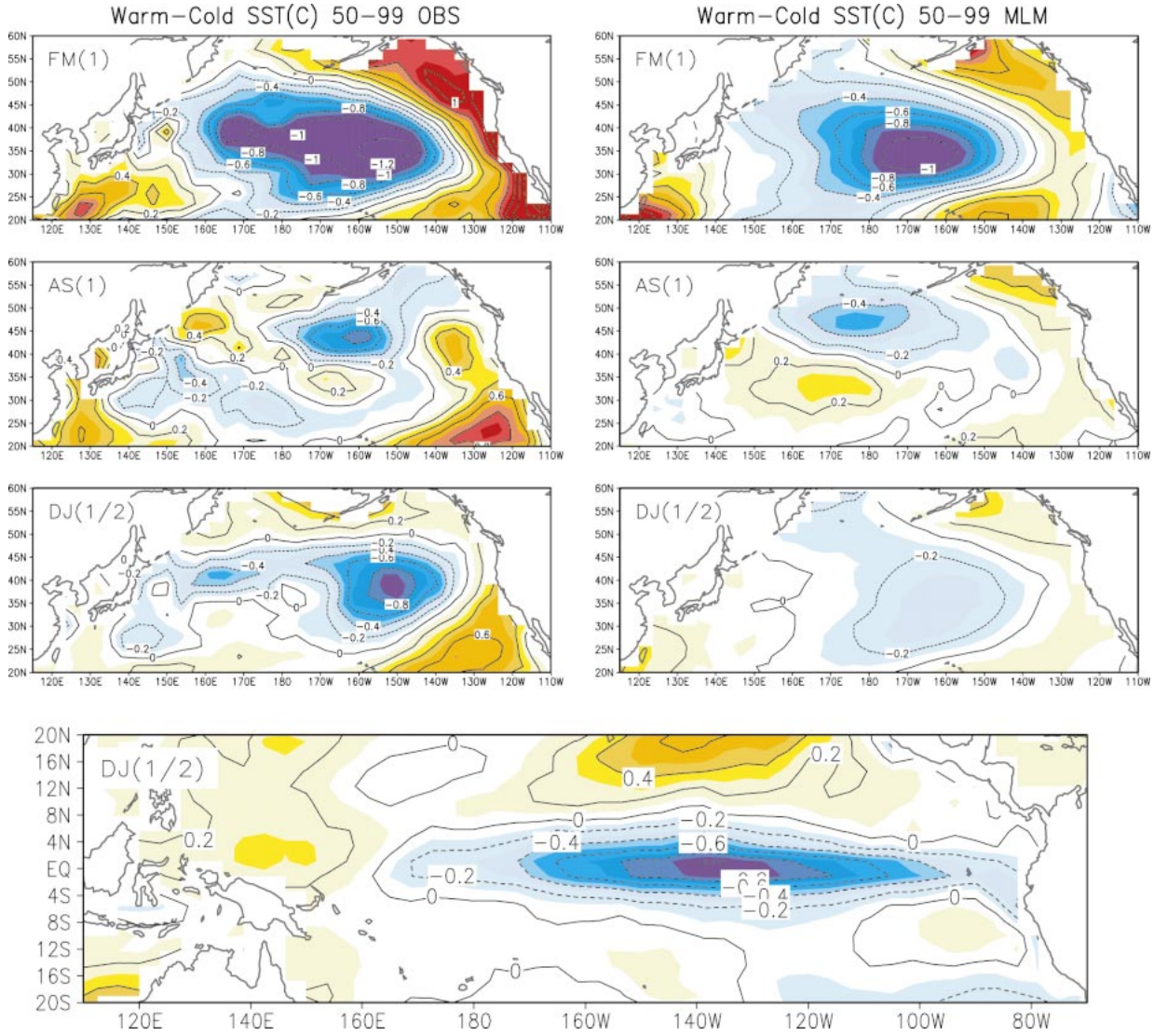

FIG. 10. El Niño − La Niña composite of SST over the North Pacific in Feb(1)–Mar(1), Aug(1)–Sep(1), and Dec(1)–Jan(2) from (left) observations and (right) the ensemble mean MLM. (bottom) The observed El Niño − La Niña composite SST in the tropical Pacific in Dec(1)–Jan(2). The shading (contour) interval is 0.1 (0.2) °C.

vening summer. They speculated that temperature anomalies that form at the surface and spread throughout the deep winter mixed layer remain beneath the mixed layer when it shoals in spring. The thermal anomalies are incorporated into the stable summer seasonal thermocline (30–100 m) and thereby insulated from surface fluxes that generally act to damp the original SST anomalies. When the mixed layer deepens again in the following fall, the anomalies are reentrained into the surface layer and influence SST. Alexander and Deser (1995) showed that this ''reemergence mechanism'' occurs at several locations away from strong ocean currents. Bhatt et al. (1998), Alexander et al. (1999), and Watanabe and Kimoto (2000) found evidence for large-scale reemergence of SST anomalies over the North Atlantic and Pacific Oceans.

Here we explore whether North Pacific SST anomalies accompanying ENSO in late winter of Yr(1) recur in the following fall/winter without persisting through the intervening summer. Bimonthly maps of the observed and simulated composite SST anomalies over the North Pacific for FM(1), AS(1) and DJ(1/2) are shown in Fig. 10. The strong basin-wide SST anomalies in FM(1) weaken and in some areas reverse sign during AS(1), but then return to a pattern in DJ(1/2) that resembles the one in the previous winter. Indeed, the pattern correlation of SST anomalies over the North Pacific between FM(1) and AS(1), is only 0.43 (0.22) in the observations (MLM) but then increases to 0.65 (0.86) between FM(1) and DJ(1/2). In nature, the recurrence of SST anomalies from one winter to the next appears strongest to the south of Alaska and in the central Pacific

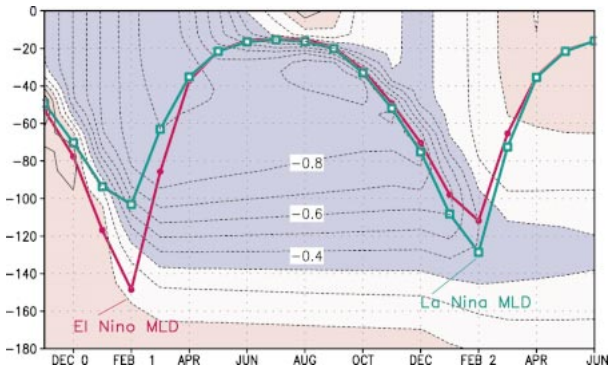

FIG. 11. The composite El Niño − La Niña ocean temperature from Nov(0) to Jun(2) and the composite MLD (m) during El Niño (solid red line) and La Niña (solid green line) from the MLM in the central North Pacific region.

(30°–35°N, 180°–150°W). Recurrence of SST anomalies is also apparent in the MLM, but the magnitude of the recurring anomalies is weaker than observed and there is some tendency for persistence of SST anomalies through summer in the Gulf of Alaska. Persistence of SST anomalies in the eastern subtropical Pacific occurs through the entire year following an ENSO event, especially in nature.

Could the SST anomalies in the North Pacific during fall/winter following an El Niño or La Niña event be forced by concurrent SST anomalies in the equatorial Pacific, rather than by the reemergence mechanism? The bottom panel in Fig. 10 shows that the SST anomalies in the equatorial Pacific have reversed sign one year after ENSO peaks, so that the atmospheric bridge would tend to create North Pacific SST anomalies opposite to those that occur in the DJ(1/2) composite. The tropical anomalies in DJ(1/2), which represent the biennial component of ENSO, are ~1/5 as large as those in the previous winter and thus have a modest effect on the North Pacific.

The simulated evolution of the composite El Niño − La Niña temperature difference averaged over the central North Pacific region (defined in section 6) is shown in Fig. 11. Results are presented from Dec(0) to Jun(2) over the upper 180 m of the ocean. Negative temperature anomalies, created in Jan(1)–Apr(1), extend over the relatively deep winter mixed layer (>100 m). While the negative SST anomalies decrease at the surface to near zero by Aug(1), the cold water is maintained beneath the ~20 m deep mixed layer through summer. As the mixed layer deepens in the following fall, water in the summer seasonal thermocline is reentrained into the surface layer, thereby cooling the SST through Jan(2).

The composite evolution of MLD in the central North Pacific region during both El Niño and La Niña events is also shown in Fig. 11. Relative to La Niña, the mixed layer is deeper as well as colder during Dec(0)–Apr(1) of El Niño events. The SST and MLD changes during winter of Yr(0/1) are inversely related, since surface heat fluxes that create negative SST anomalies also lead to enhanced convective mixing and thus positive MLD anomalies. In contrast, the SST and MLD anomalies are positively correlated in the winter of Yr(1/2): anomalously cold water is associated with a shallower mixed layer. Alexander et al. (2001) found that this reversal in the SST–MLD relationship results from the seasonal cycle of MLD and the reemergence process. When the deep winter mixed layer shoals, the water left behind subsequently affects the density profile in the seasonal thermocline. When the winter mixed layer is colder (and/or saltier) than normal, the vertical stratification is enhanced in the seasonal pycnocline. As a result, the penetration depth of the mixed layer will decrease for the same amount of surface forcing, especially during the main period of deepening in the following fall and winter. Thus, the negative SST anomaly formed during El Niño (La Niña) winters leads to negative (positive) MLD anomalies in the following fall/winter.

8. Oceanic feedback on the atmospheric bridge

Given the influence of the atmospheric bridge on the global oceans, to what extent do the remote ENSO-related SST anomalies feed back upon the atmosphere? Previous studies have focused on how regional air–sea interaction influences the atmospheric bridge—for example, how North Pacific SST anomalies influence the atmospheric response to ENSO in the PNA region. Here, we examine how global as well as regional air–sea coupling impacts this response. Nonlocal air–sea interaction can affect the response via ''multiple bridges''; for instance, ENSO-related SST anomalies that develop in the Indian Ocean, western Pacific, or other ocean basins can subsequently influence the atmosphere over the PNA region.

a. Previous results

Hendon and Hartmann (1982) suggested that the extratropical atmospheric response to ENSO is weakened by the presence of an ocean, which thermally damps the atmosphere via surface heat fluxes. This damping is reduced if the SSTs are allowed to adjust to the overlying atmosphere, so that low-level low-frequency thermal variance is enhanced in a coupled atmosphere–ocean model compared to a model with fixed climatological SSTs (Barsugli 1995; Manabe and Stouffer 1996; Bladé 1997, 1999; Barsugli and Battisti 1998; Saravanan 1998). Several of these studies found that ''reduced thermal damping'' increases the variance and persistence of certain atmospheric circulation anomalies but the reasons why particular patterns are enhanced is unclear.

Frankignoul (1985), Robinson (2000), and Kushnir et al. (2002, this issue) discuss other physical mechanisms by which midlatitude SST anomalies influence the atmosphere, including Rossby wave propagation

from the associated low-level heat source/sink (e.g., Hoskins and Karoly 1981), stationary waves driven by large-scale changes in precipitation (e.g., Rodwell et al. 1999), storm track changes that affect the large-scale flow (e.g., Ting and Peng 1995), and changes in the mean climate due to air–sea coupling (Robinson 2000).

The more specific question of how extratropical air–sea coupling influences ENSO teleconnections in the PNA region has been examined by Alexander (1992b), Bladé (1999), and Lau and Nath (1996, 2001) using sets of atmospheric GCM simulations in which the atmosphere is forced with observed or idealized ENSO SST boundary conditions in the tropical Pacific. The impact of the extratropical ocean on the atmospheric response to ENSO was assessed by comparing ''uncoupled simulations,'' in which climatological SSTs were prescribed outside the tropical Pacific, with ''coupled'' simulations, in which the atmosphere was allowed to interact with a mixed layer ocean model. However, the location of the tropical SST forcing, the mixed layer domain and physics, and the treatment of the seasonal cycle, differed from one experiment to another.

The studies by Alexander, Bladé, and Lau and Nath reached different conclusions. For instance, using an ensemble of five simulations with an idealized ENSO event specified in the Community Climate Model [(CCM) version 0A, an AGCM from NCAR with R15 resolution], Alexander (1992b) found that midlatitude air–sea feedback damped the anomalous upper-level winter circulation in the PNA sector. Bladé (1999) reached a similar conclusion, using long perpetual January integrations of the R15 GFDL GCM and synthetic tropical SSTs. In contrast, Lau and Nath (1996) found that coupling greatly enhanced the winter near-surface ENSO-related atmospheric anomalies (temperature, humidity, and wind speed) in the PNA region and, to a lesser extent, the upper-level response. Their results were obtained from an ensemble of four integrations with the R15 GFDL model forced with observed tropical SSTs for the 1946–88 period. In Bladé's study, only the low-level temperature response was amplified in the presence of coupling with increased persistence of the response evident at lags of 3–6 months, consistent with reduced thermal damping. In these studies, however, differences between the coupled and uncoupled upper-level circulation were not always statistically significant. Furthermore, models with R15 or similarly coarse resolution underestimate tropical precipitation and storm track variability, usually resulting in a weaker atmospheric response to both tropical and midlatitude SST anomalies.

Lau and Nath (2001, hereafter LN) repeated their series of four-member ensemble experiments using the R30 GFDL model for the 1950–95 period. They found that the differences between the coupled and uncoupled response over the Northern Hemisphere depended on the seasonal cycle and the polarity of ENSO events. For El Niño events, coupling did not modify the amplitude of the 500-mb height anomalies during the peak in response to ENSO that occurs in Jan(1)–Feb(1) (hereafter JF), but for La Niña events, it doubled the amplitude of the JF anomalies over the PNA sector. This apparent nonlinearity in the impact of midlatitude coupling, with positive oceanic feedback occurring only in the presence of positive midlatitude SST anomalies, is consistent with the lack of sensitivity of AGCMs to negative midlatitude SST anomalies (Kushnir et al. 2002). On the other hand, because LN's mixed layer extends to all oceans outside the tropical Pacific, the coupled response could be influenced by multiple bridges in addition to local air–sea coupling.

Newman et al. (2000) diagnosed the midlatitude ocean–atmosphere interactions in LN's coupled experiment using a linear inverse modeling (LIM) technique (e.g., Penland and Sardeshmukh 1995). Their results suggest that the linear feedback of extratropical SSTs upon the atmosphere is weak and enhances the local atmospheric thermal variability, in agreement with Barsugli and Battisti (1998). The feedback also appears to damp barotropic variability in the central North Pacific, which concurs with Alexander's and Bladé's findings.

With the exception of Bladé's (1999) study, the model experiments discussed above were based on a relatively small number of realizations, so discrepancies among them may simply be due to sampling variability. Given that the response to prescribed midlatitude SSTs is modest in most recent AGCM experiments (Kushnir et al. 2002), this suggests that large ensembles and/or long integrations are necessary to resolve the effect of midlatitude oceanic feedback on the atmosphere. Moreover, the 50-m slab ocean employed by Bladé and Lau and Nath does not accurately represent ocean conditions in late winter, since the observed MLD exceeds 100 m in the central North Pacific and most of the North Atlantic from January to March (e.g., Monterey and Levitus 1997).

b. Revisiting the effect of coupling on the extratropical ENSO response

We have performed model experiments with larger ensembles and improved mixed layer physics to address sampling variability issues and to examine the relative roles of local and remote air–sea feedback on ENSO teleconnections. In addition to the MLM experiment, two complementary sets of ensemble integrations, the control and NP–MLM experiments, have been conducted. Recall from section 2 that all three experiments have the same SST forcing in the eastern tropical Pacific, but the MLM has an interactive model over the remainder of the global ocean, the NP–MLM has an interactive ocean only in the North Pacific (north of 21°N) and the control has no interactive ocean. At the outset, the expectation is that differences between the NP–MLM and control responses can be attributed to local coupling effects in the North Pacific, whereas dif-

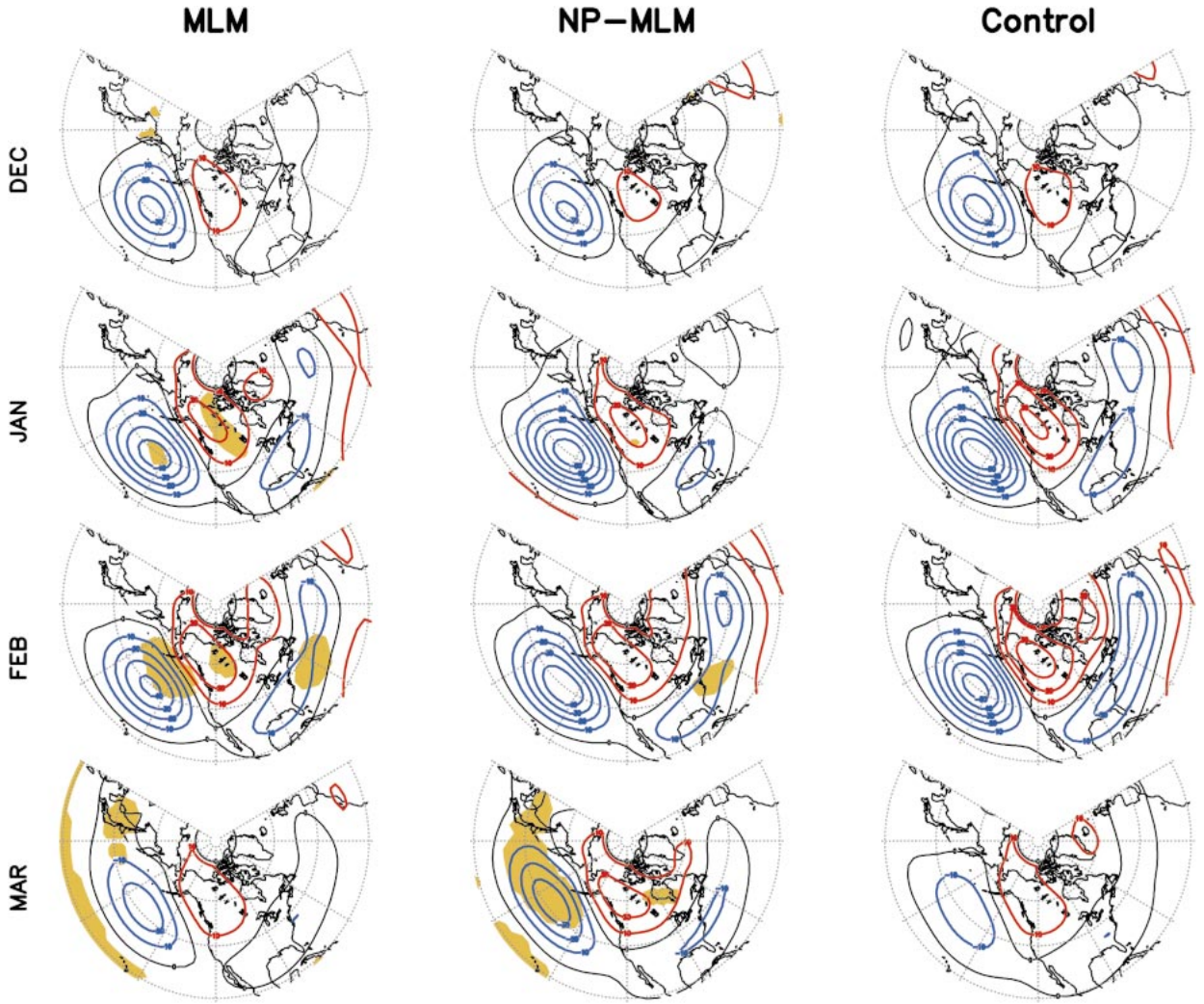

FIG. 12. Regression coefficients of monthly mean 500-mb height anomalies vs the Jan ENSO index from the previous Dec to the following Mar, for the MLM, NP–MLM, and control experiments. Contour interval is 10 m; positive (negative) contours are red (blue). The shading indicates two-tailed 95% statistical significance of the difference between coupled and uncoupled regressions.

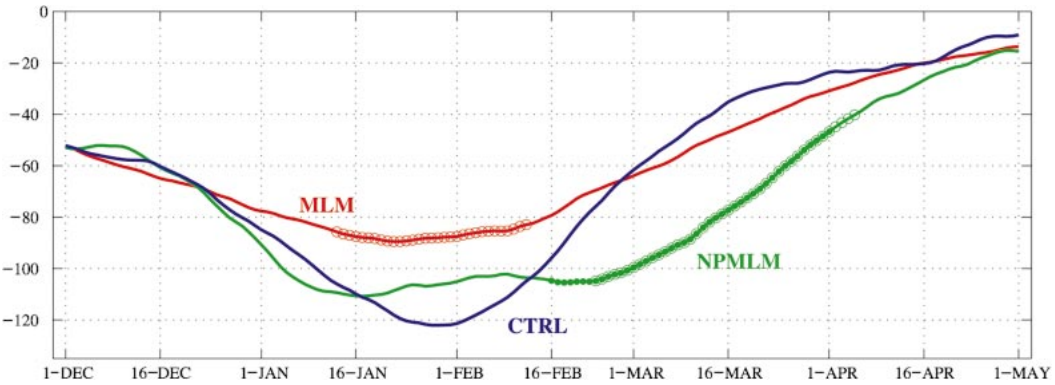

FIG. 13. Time series of the warm − cold composite of the 30-day running mean 500-mb height anomalies averaged over a box centered in the North Pacific (32°–48°N, 176°E–142°W) for all three experiments. Open circles indicate 95% significance of the differences between the anomalies in MLM or NP–MLM and the control, while full circles indicate significant differences between anomalies in the NP–MLM and MLM.

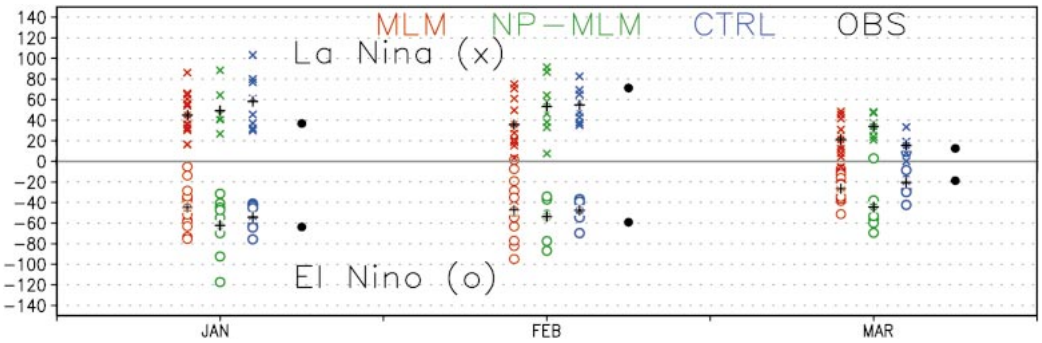

FIG. 14. Warm (El Niño) and cold (La Niña) composites of monthly mean 500-mb North Pacific height anomalies in all three experiments (averaged over the same box as in Fig. 13), for all members in each experiment during Jan, Feb, and Mar of Yr(1). The black crosses indicate the ensemble averages, while the black circle indicates the observed composite value.

ferences between the MLM and NP–MLM are due to air–sea coupling outside the North Pacific.

The extratropical atmospheric response to ENSO is examined using regression and composite analyses. The statistical significance of the difference in these quantities between experiments is estimated using Monte Carlo methods (e.g., Wilks 1995), as follows. The regression (or composite) values from the individual simulations of the experiments being compared are pooled together. At each grid point, 6000 pairs of random ensemble averages are constructed allowing for replacement. Differences between pairs of ensemble averages selected from this pool are then used to generate a near-normal distribution of values. The difference between experiments is deemed to be significant at the 95% level if the magnitude of the actual value exceeds the top or bottom 2.5% of the Monte Carlo distribution values. In general, traditional Student's *t* tests produce similar results to those shown here.

The evolution of the atmospheric response to ENSO during the winter months, illustrated by linearly regressing monthly mean 500-mb heights against the January ENSO index (Fig. 12), is broadly similar in the three experiments. The tropically forced wave train arches across the North Pacific, North America, and the North Atlantic, with maximum amplitude in JF. The JF height anomalies throughout the PNA sector are weaker in the MLM experiment relative to the control. The damping effect of global coupling from mid-January to mid-February is more clearly evident in Fig. 13, which shows the time evolution of the 30-day running mean warm − cold composite of the height anomaly averaged over the North Pacific (32°–48°N, 176°E–142°W). Alexander (1992b), Bladé (1999), and Newman et al. (2000) also found that coupling slightly damped ENSO-related atmospheric anomalies over the North Pacific in winter. Similar results are also seen in other fields, such as SLP and 200-mb zonal wind (not shown).

Differences between the midwinter response to ENSO in the NP–MLM and control experiments are modest and do not pass the significance test at the 95% level (Figs. 12 and 13). More striking is that the wave train in the NP–MLM is strongly enhanced relative to the control and MLM experiments in March. The anomaly centered over the northeastern Pacific in March is also enhanced in the MLM relative to control but this difference is small and not significant at the 95% level. The North Pacific height anomaly expands toward the west from February to March in both the MLM and NP–MLM simulations.

While coupling appears to influence the mean response, does it impact the distribution of the response, that is, how does the anomaly vary among ensemble members? Does the impact of coupling differ between warm and cold events? Do the observed anomalies lie within the model spread? To address these questions, the warm and cold composite 500-mb North Pacific height anomaly for each ensemble member in the three experiments and observations as well are shown in Fig. 14. There is a large amount of spread among ensemble members, and by eye there are notable differences in the distributions between experiments. However, we cannot determine if the ensembles being compared are significantly different from each other by visual inspection; that is, they could be subsamples from the same underlying distribution. To test if the difference between ensemble distributions is significant, we use the nonparametric two-sample Kolmogorov–Smirnov measure, D_{ks}, the maximum difference between the cumulative distribution functions of the ensembles being compared (Kendall and Stewart 1977; also see the appendix in Sardeshmukh et al. 2000).

The warm and cold composite distributions can only be distinguished from each other at the 95% confidence level for the MLM experiment in February and the NP–MLM experiment in March. Thus, we refrain from a discussion of nonlinearity in the response to ENSO and how coupling might impact it. The MLM differs from the other two experiments at the 95% level for warm − cold composites in January and for cold events in February. The warm and cold NP–MLM distributions differ from both the MLM and control distributions at the 99%

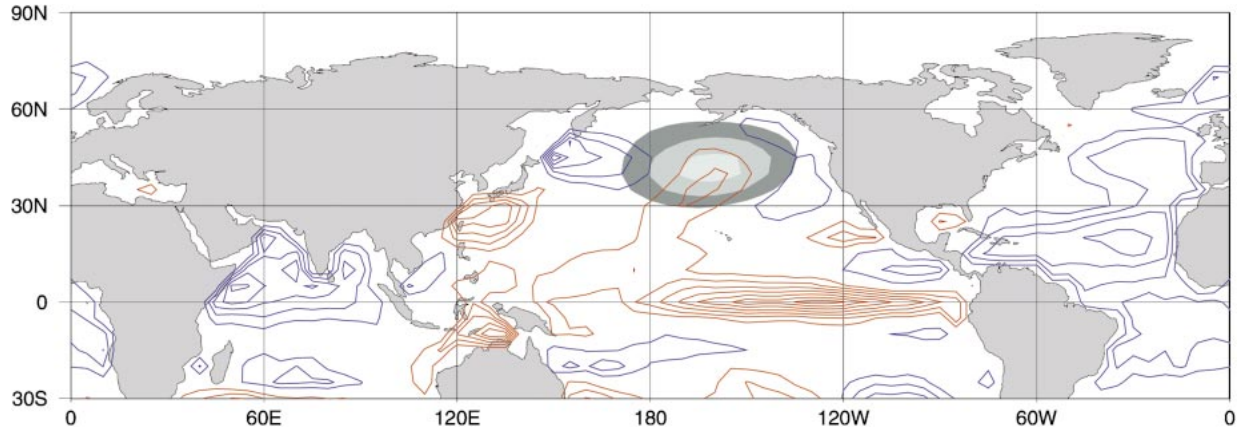

FIG. 15. Sensitivity map, or influence function, of a negative height anomaly over the North Pacific to anomalous SSTs 60 days earlier in the MLM. The influence function is contoured at an interval of 0.002 K m^{-1}; the zero contour is removed for clarity and positive (negative) values are red (blue). The target height response at 200 mb is indicated by gray shading with a 0.25-m interval.

confidence level in March. However, the observed March composite value lies beyond the NP–MLM distribution for La Niña events and is smaller than all but one NP–MLM member for El Niño events. In contrast, the observed values lie well within the distributions of the other experiments, suggesting that a crucial damping process coming from other ocean basins is missing in the NP–MLM experiment in late winter.

The impact of multiple bridges upon the North Pacific height anomaly in the MLM experiment is diagnosed using an ''influence function'' (Branstator 1985; Newman and Sardeshmukh 1998). The influence function (**g**) can be thought of as an inverse Green's function. That is, rather than showing how the response at all locations is affected by a specified source of forcing, **g** shows how the forcing from all locations affects a specified response. Here, **g** represents the sensitivity of a target atmospheric response, specified as a barotropic height anomaly over the central North Pacific, to prior global SST anomalies. This sensitivity is determined using lagged multiple linear regression applied to the November–March MLM output (see the appendix for more details). Note that the height response depends not only on the influence function but also on the actual pattern of the anomalous SSTs: a region will have a substantial impact on the response only if both **g** and the ENSO-induced SST anomalies are large in that region.

The sensitivity of a negative height anomaly over the central North Pacific (a deeper Aleutian low) in winter to anomalous SST 60 days earlier is shown in Fig. 15; qualitatively similar results are obtained for shorter or longer lags. As expected, the largest negative (positive) North Pacific height response can be generated by anomalously warm (cold) SSTs in the equatorial Pacific. To a lesser degree, the height anomaly is also sensitive to local SST forcing: a warm (cold) SST anomaly in the central North Pacific (~35°N, 160°W) strengthens (weakens) the trough 60 days later, as would a cold (warm) SST anomaly along the west coast of North America. Since the SST anomalies associated with the bridge in the eastern half of the North Pacific (Fig. 6b) are opposite to **g** (Fig. 15), local air–sea interaction appears to weakly damp the direct atmospheric response to ENSO.

The bridge induces SST anomalies of the same sign as those in the eastern equatorial Pacific throughout most of the tropical oceans, particularly in the Indian and Atlantic basins (Fig. 6). The influence function indicates that SST anomalies in these basins force a North Pacific height response opposite to that forced by eastern tropical Pacific SST anomalies. The sensitivity of height anomalies in the PNA sector to Indian Ocean SST anomalies is consistent with simulations in which SST were specified in the Indian Ocean in the NCEP AGCM (Kumar and Hoerling 1998; Barsugli and Sardeshmukh 2002) and in the CCM3 (M. P. Hoerling 2002, personal communication). The sensitivity to conditions in the tropical Atlantic Ocean, while unexpected, is supported by recent CCM simulations in which SST anomalies are specified only in the tropical Atlantic (R. Saravanan 2002, personal communication). The absence of coupling in the tropical Indian and Atlantic Oceans, and thus the absence of damping from these regions, may explain the stronger wintertime response in the NP–MLM relative to the MLM experiment (Figs. 12 and 13).

The dipole in **g** near Japan (Fig. 15) implies that changes in the SST gradient across the Kuroshio Current extension forced by the bridge (Fig. 6) amplify the North Pacific height anomaly. AGCM experiments conducted by Peng et al. (1997) and Yulaeva et al. (2001) also suggest that conditions in the western North Pacific Ocean can influence the atmospheric circulation in the PNA region. Monthly SST anomalies near Japan do not reach significant amplitude until late winter and early spring (not shown, but compare the DJF and MAM panels in Fig. 6), while the central North Pacific SST anomaly is well established earlier in the winter. Thus,

the net feedback from the Pacific north of 21°N could result in damping of the height anomaly during midwinter, but weaker damping and perhaps even amplification by late winter and early spring, which is consistent with the differences between the NP–MLM and control experiments (and to a lesser degree the MLM and control) in Figs. 12 and 13. Note that the relationship between anomalous SST and the atmospheric height anomalies also exhibits month-to-month variations (Newman and Sardeshmukh 1998; Wang and Fu 2000) not considered here.

c. Discussion

Our results suggest that the impact of air–sea coupling on the extratropical atmospheric response to ENSO is complex. Both local and remote air–sea interaction influence ENSO teleconnections over the PNA region and coupling effects vary with the seasonal cycle. The net effect of global coupling on the ENSO response in the PNA sector is smaller than both the ENSO signal forced directly from the eastern Pacific and internal atmospheric variability (Fig. 14), which implies that very large ensembles are needed to determine the full effect of air–sea interaction on the response to ENSO at subseasonal timescales (Sardeshmukh et al. 2000).

The net global effect of coupling may be modest, however, because larger atmospheric responses to SST anomalies in separate areas partly cancel over the PNA region. Since the global SST anomaly pattern resulting from multiple bridges varies from event to event, the net effect of coupling will also differ. Thus, to better understand the full atmospheric response to ENSO and to simulate the response during individual ENSO events will require GCMs to correctly model a series of processes including: the SST evolution in the Indian, Atlantic, and North Pacific Oceans, the local atmospheric response to these SST anomalies, and the teleconnections from these regions to the PNA sector.

Given the complexity of the model results, the physical mechanisms responsible for the ocean-to-atmosphere feedback during ENSO events are not readily apparent and likely involve both tropical and extratropical processes. Air–sea interaction might influence the extratropical height response to ENSO via changes in tropical precipitation. The warm − cold composite precipitation in both coupled experiments minus the control during Feb(1) and the evolution of the precipitation anomalies in the central and western equatorial Pacific for all three experiments are shown in Fig. 16. Coupling decreases the tropical precipitation associated with ENSO in midwinter by reducing the amplitude of precipitation anomalies over the central and western equatorial Pacific (Fig. 16c). Surprisingly, this signal is present even in the NP–MLM experiment, along with corresponding changes in the 200-mb zonal winds (not shown), even though the SST boundary conditions south of 20°N are identical in the NP–MLM and control experiments.

The reduced precipitation in the central equatorial Pacific in the coupled experiments during JF weakens the diabatic forcing of the extratropical atmospheric circulation. The enhanced precipitation over 0°–10°N in the Indian Ocean and the reduced precipitation near the Philippines in the MLM relative to the NP–MLM (not shown but cf. Figs. 16a and 16b) are qualitatively similar to changes in the forcing necessary to further weaken the extratropical wave train (e.g., Ting and Sardeshmukh 1993). The difference in the precipitation/circulation over the tropical Pacific between the NP–MLM and control experiments is unexpected and may be due to insufficient sampling. However, the difference between the precipitation between the NP–MLM and control experiments is statistically significant in the central and western equatorial Pacific. Air–sea coupling in the North Pacific (including the subtropics) could influence tropical precipitation through processes that span from the midlatitudes to the Tropics, such as cold surges that propagate from Asia to the western equatorial Pacific.

In addition to changes in tropical forcing, differences between the experiments may result from extratropical processes. For example, reduced thermal damping could contribute to the enhancement of the NP–MLM response relative to the control in March. Indeed, the loss of energy from the atmosphere to the ocean via surface heat fluxes is 20%–30% weaker by February in the NP–MLM experiment (not shown, but see Figs. 4–12 in Lau and Nath 1996), consistent with the slow adjustment of midlatitude SST anomalies to the overlying atmosphere. However, the ENSO-related SST anomalies in the North Pacific are also driven by anomalous low-level winds, which are not considered in the reduced thermal damping paradigm. The sensitivity of central North Pacific heights to SST changes near Japan (Fig. 15) suggests that changes in the storm track could also be relevant. In March, precipitation just south of Japan and transient eddy flux convergence over the west Pacific are enhanced in the NP–MLM relative to the control (not shown). While these differences in storm track parameters are significant at the 99% and 95% levels, respectively, it is not yet clear whether the changes in the transient eddies caused or resulted from the large-scale circulation anomalies.

Finally, we note that one advantage of our experimental design compared to coupling an AGCM to an OGCM is that, by construction, SST anomalies are realistic in the ENSO region. Recent research (Pierce et al. 2000; Vimont et al. 2001), however, has suggested that winds in the extratropics may affect the development of tropical SST anomalies, a potentially important feedback missing from our experiments.

d. Oceanic feedback in other locations

While we have focused on the impact of air–sea interaction in the ENSO response in the PNA sector, air–

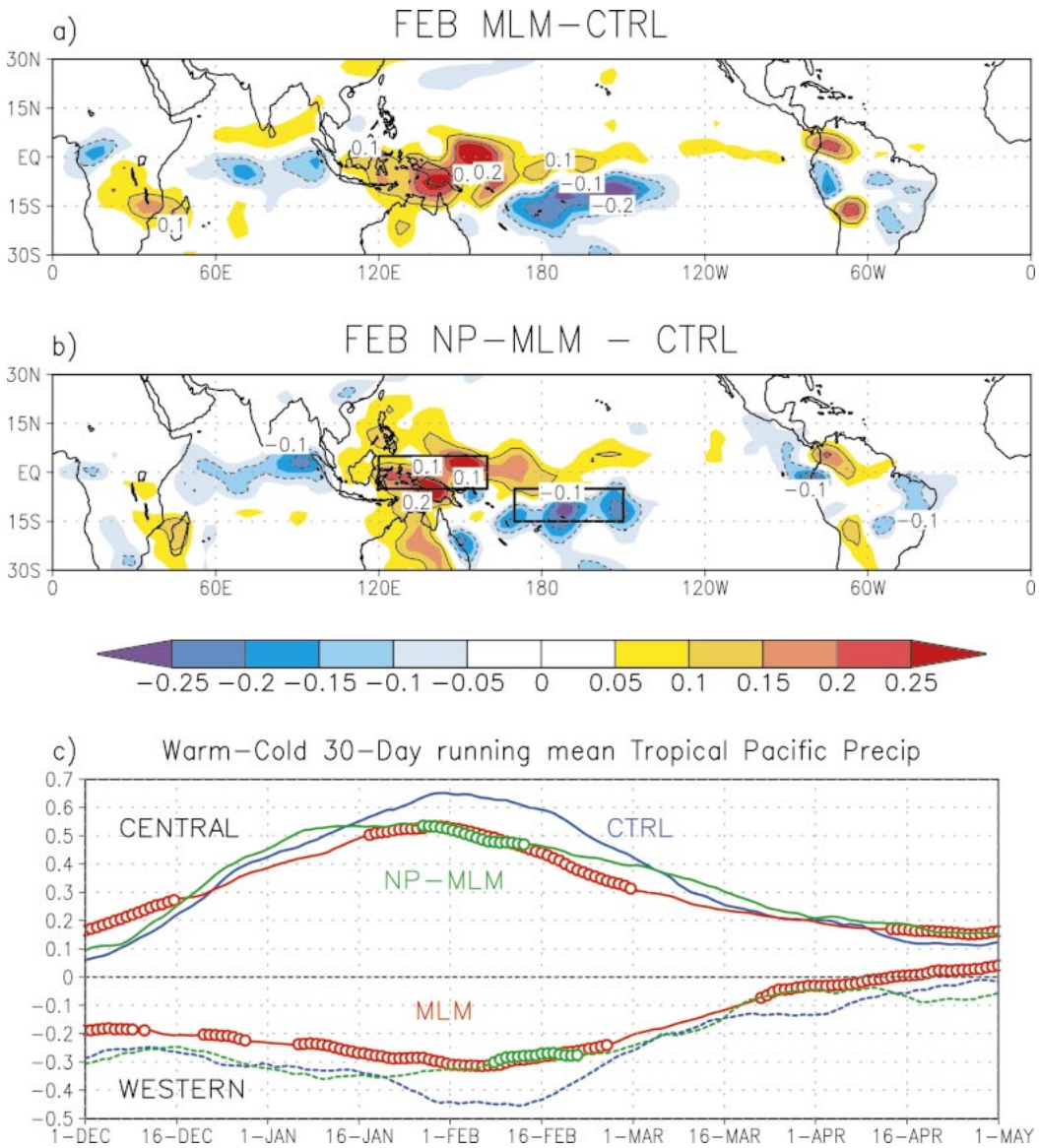

FIG. 16. (a) MLM minus control and (b) NP–MLM minus control warm − cold composite tropical precipitation during Feb(1). Contour (shading) interval is 0.1 (0.05) cm day^{-1}. (c) Warm − cold composite of the 30-day running mean precipitation (cm day^{-1}) in the MLM, NP–MLM, and control experiments averaged over the regions shown in (b): the central (5°–15°S, 170°E–150°W) and western (5°S–5°N, 120°–160°E) equatorial Pacific. Precipitation anomalies in the central (western) Pacific are shown by solid (dashed) lines; open circles indicate that the differences between the anomalies in the MLM or NP–MLM and the control are significant.

sea feedback influences the atmospheric bridge in other regions as well. Wang et al. (2000) proposed that a strong anticyclone that forms to the east of the Philippines during El Niño winters creates cold SST anomalies near 10°N, 140°E via evaporative cooling and enhanced entrainment. These cold SSTs reinforce the anticyclone, enabling it to persist for several months. By comparing the local atmospheric response in a coupled and an uncoupled simulation, Lau and Nath (2000) found that the ENSO-related SST anomalies in the Indian Ocean tend to enhance (reduce) the precipitation and flow in the summer Asian monsoon, in opposition to the direct response to warm (cold) SST anomalies in the tropical Pacific Ocean.

9. Outstanding issues

The full extent of the atmospheric bridge spans several different processes, including the following: the global atmospheric response to ENSO SST anomalies; the resulting changes in heat, momentum, and freshwater fluxes across the air–sea interface outside of the equatorial Pacific; the ocean's response to these surface flux anomalies, including changes in SST, MLD, and

salinity; and the feedback of the remote SST anomalies onto the atmosphere. While considerable progress has been made in our understanding of each of these subtopics, several outstanding issues remain.

A detailed discussion of unresolved issues concerning the atmospheric response to tropical SST anomalies can be found in section 6 of Trenberth et al. (1998). Of relevance here is how the large-scale atmospheric changes associated with ENSO are communicated to the surface via changes in solar radiation, precipitation, and boundary layer processes, which are not well simulated in AGCMs. Perhaps the most important requirement, in terms of improved simulation of the ENSO-related SST anomalies, is a better representation of clouds and their influence on solar radiation.

Most studies that have examined the remote oceanic response to ENSO have focused on SST anomalies in the Northern Hemisphere during winter. Relatively large ENSO-related SST anomalies in the Southern Hemisphere during winter and in the North Pacific during summer have received much less attention. Questions also remain about the Indian Ocean response to ENSO; while most studies have found a basinwide warming in Dec(0)–May(1), it is not clear how much of the east–west SST dipole that develops along the equator in boreal fall is also due to the atmospheric bridge. In addition, the remote influence of ENSO on other ocean fields such as mixed layer depth, and temperature, salinity, and currents as a function of depth requires further study.

A complete picture of the climate system response to ENSO should incorporate both the atmospheric bridge and the dynamical ocean response to tropical SST anomalies. Kelvin and other coastally trapped ocean waves generated by ENSO clearly influence SST along the west coast of North and South America. Baroclinic Rossby waves are generated by the passage of these waves and by changes in wind stress curl associated with atmospheric teleconnections, especially variations in the Aleutian low (Pares Siera and O'Brien 1989; Jacobs et al. 1994; Miller et al. 1997). Since baroclinic Rossby waves take approximately 5–10 years to cross the North Pacific, dynamical ocean processes are important in slow basinwide thermocline changes and may influence SST anomalies at low frequencies. Wind and buoyancy driven changes in the ocean circulation may also result from the atmospheric response to low-frequency changes in SST in the equatorial Pacific. In principle, coupled GCMs can be used to assess the roles of the atmosphere and oceans in the global response to SST anomalies in the equatorial Pacific, provided the models have a reasonable representation of ENSO.

Perhaps the most outstanding issue concerning the atmospheric bridge is the extent to which and by what means SST anomalies beyond the equatorial east Pacific feed back on the atmosphere. The effect of midlatitude air–sea feedback on the atmospheric circulation during ENSO has differed among previous modeling studies. The GCM simulations we have performed suggest that global air–sea interaction damps the midwinter response to ENSO in the PNA region while air–sea interaction in the North Pacific strengthens the response in March. However, several questions remain. Are both signals robust and reproducible in other models? If so, what physical processes are responsible? Is reduced thermal damping, which enhances persistence of atmospheric anomalies (e.g., Barsugli and Battisti 1998) critical, and/or are dynamical changes, perhaps a change in the intensity or location of the storm tracks, important as well? How does air–sea interaction, including interactions in the North Pacific, influence tropical precipitation? Does reemergence of ENSO-related SST anomalies in the following fall/winter affect the atmosphere? How does air–sea interaction during ENSO in other locations, for example, the tropical Atlantic, Indian Ocean, and Southern Hemisphere influence the atmospheric response to ENSO? More definitive answers to these questions require a very large ensemble of coupled and uncoupled simulations.

Acknowledgments. We thank Mary Jo Nath and Christopher Winkler for their assistance in analyzing and graphing the results. Comments by Robert Scott and two anonymous reviewers along with conversations with Gil Compo and Joe Barsugli helped to improve the manuscript. Tom Smith from NCEP provided the SSTs used as boundary conditions in the model simulations.

APPENDIX

Empirical Influence Functions

The linear evolution of an anomaly vector $\mathbf{x}(t)$ over a time interval $[t, t + \tau]$ can be expressed as

$$\mathbf{x}(t + \tau) = \mathbf{G}(\tau)\mathbf{x}(t) + \mathbf{s}(t + \tau), \tag{A1}$$

where $\mathbf{G}(\tau)$ is a linear operator (or propagator) matrix and $\mathbf{s}(t + \tau)$ is the corresponding error vector. Here $\mathbf{G}(\tau)$ can be determined from the zero-lag and time-lag covariability statistics of $\mathbf{x}(t)$ in a least squares sense (e.g., Wilks 1995) using multiple linear regression (MLR). Now suppose we are interested in a particular pattern of the response to prior anomalous initial conditions, say the height anomaly over the North Pacific that results from anomalous SST forcing 60 days earlier. Let $\mathbf{w}$ be a vector that represents this response of interest. Then a measure of the magnitude of this response is the projection of $\mathbf{w}$ on the total field $\mathbf{x}(t + \tau)$, or

$$R = \mathbf{w}^{\mathrm{T}}\mathbf{x}(t + \tau). \tag{A2}$$

From (A1) and (A2) the expected response for a given initial state $\mathbf{x}(t)$ is

$$\langle R \rangle = \mathbf{w}^{\mathrm{T}}\mathbf{G}(\tau)\mathbf{x}(t), \tag{A3}$$

where the brackets indicate an ensemble average so that $\langle \mathbf{s} \rangle = 0$. Thus, the sensitivity of the response $\mathbf{w}$ to initial

conditions in any location can be determined from (A3) as

$$\mathbf{g}^{\mathrm{T}} = \mathbf{w}^{\mathrm{T}}\mathbf{G}(\tau). \quad \text{(A4)}$$

An element of this sensitivity map, or influence function $\mathbf{g}(\theta, \lambda)$, is the contribution to the target response from a point with unit initial condition located at latitude θ and longitude λ.

The influence function shares two notable similarities with the Green's function. First, convolving **g** with an actual pattern of SST forcing at any given time will produce a corresponding height response. Second, **g** measures the cumulative effect of forcing over the time interval τ. For example, a point source of anomalous SST in the Tropics may directly produce a North Pacific height response, but it may also induce anomalous SST in other locations that could in turn further enhance or reduce the height anomaly.

In this analysis, we apply MLR to the anomaly vector defined as

$$\mathbf{x} = \begin{bmatrix} \mathbf{T} \\ \mathbf{Z}_{850} \\ \mathbf{Z}_{200} \end{bmatrix},$$

where **T** is the anomalous SST subvector, and $\mathbf{Z}_{200}$ and $\mathbf{Z}_{850}$ are 200- and 850-mb geopotential height anomaly subvectors. Data north of 30°S are interpolated to a 5° × 5° grid. Anomalies are determined during NDJFM as departures of daily values from an annually varying climatology, where the climatology is defined as both a time and ensemble mean. Anomalies are then filtered with a 30-day running mean. Finally, anomalies are truncated in EOF space to the 40 leading geopotential height and SST EOFs. This truncation retains more than 80% of domain-integrated variance for each field. A lag of 20 days is used to compute $\mathbf{G}(\tau)$, as $\mathbf{G}(\tau) = [\mathbf{G}(20)]^{\tau/20}$. Results are not qualitatively sensitive to either truncation or lag. Apart from sampling, results are also similar if we compute $\mathbf{G}(\tau)$ from other lags; for example, $\mathbf{G}(60) = [\mathbf{G}(20)]^3 = [\mathbf{G}(30)]^2$, suggesting that the evolution of **x** can be described by a simple linear dynamical equation (Winkler et al. 2001). Since the influence function in Fig. 15 shows sensitivity of a height response alone, the SST subvector of **w** is set to zero. In addition, only the SST portion of **g** is shown in Fig. 15, but similar maps result at 200 and 850 mb for the sensitivity of the North Pacific height anomaly to previous height anomalies.

REFERENCES

Alexander, M. A., 1990: Simulation of the response of the North Pacific Ocean to the anomalous atmospheric circulation associated with El Niño. *Climate Dyn.,* **5,** 53–65.

——, 1992a: Midlatitude atmosphere–ocean interaction during El Niño. Part I: The North Pacific Ocean. *J. Climate,* **5,** 944–958.

——, 1992b: Midlatitude atmosphere–ocean interaction during El Niño. Part II: The North Hemisphere atmosphere. *J. Climate,* **5,** 959–972.

——, and C. Deser, 1995: A mechanism for the recurrence of wintertime midlatitude SST anomalies. *J. Phys. Oceanogr.,* **25,** 122–137.

——, and J. D. Scott, 1995: Atlas of climatology and variability in the GFDL R30S14 GCM. CIRES, University of Colorado, 121 pp. [Available from the authors at NOAA–CIRES Climate Diagnostics Center, R/CDC1, 325 Broadway, Boulder, CO 80305-3328.]

——, and ——, 1997: Surface flux variability over the North Pacific and North Atlantic Oceans. *J. Climate,* **10,** 2963–2978.

——, C. Deser, and M. S. Timlin, 1999: The reemergence of SST anomalies in the North Pacific Ocean. *J. Climate,* **12,** 2419–2433.

——, J. D. Scott, and C. Deser, 2000: Processes that influence sea surface temperature and ocean mixed layer depth variability in a coupled model. *J. Geophys. Res.,* **105,** 16 823–16 842.

——, M. S. Timlin, and J. D. Scott, 2001: Winter-to-winter recurrence of sea surface temperature, salinity and mixed layer depth anomalies. *Progress in Oceanography,* Vol. 49, Pergamon, 41–61.

Barsugli, J. J., 1995: Idealized models of intrinsic midlatitude atmosphere–ocean interaction. Ph.D. thesis, University of Washington, 187 pp. [Available online at http://www.cdc.noaa.gov/~jjb/thesis.html.]

——, and D. S. Battisti, 1998: The basic effects of atmosphere–ocean thermal coupling on midlatitude variability. *J. Atmos. Sci.,* **55,** 477–493.

——, and P. D. Sardeshmukh, 2002: Global atmospheric sensitivity to tropical SST anomalies throughout the Indo-Pacific basin. *J. Climate,* in press.

Behera, S. K., P. S. Salvekar, and T. Yamagata, 2000: Simulation of interannual SST variability in the tropical Indian Ocean. *J. Climate,* **13,** 3487–3499.

Bhatt, U. S., M. A. Alexander, D. S. Battisti, D. D. Houghton, and L. M. Keller, 1998: Atmosphere–ocean interaction in the North Atlantic: Near-surface climate variability. *J. Climate,* **11,** 1615–1632.

Bjerknes, J., 1966: A possible response of the atmospheric Hadley circulation to equatorial anomalies of ocean temperatures. *Tellus,* **18,** 820–829.

——, 1969: Atmospheric teleconnections from the equatorial Pacific. *Mon. Wea. Rev.,* **97,** 163–172.

Blackmon, M. L., J. E. Geisler, and E. J. Pitcher, 1983: A general circulation model study of January climate anomaly patterns associated with interannual variation of equatorial Pacific sea surface temperatures. *J. Atmos. Sci.,* **40,** 1410–1425.

Bladé, I., 1997: The influence of midlatitude ocean–atmosphere coupling on the low-frequency variability of a GCM. Part I: No tropical SST forcing. *J. Climate,* **10,** 2087–2106.

——, 1999: The influence of midlatitude ocean–atmosphere coupling on the low-frequency variability of a GCM. Part II: Interannual variability induced by tropical SST forcing. *J. Climate,* **12,** 21–45.

Branstator, G., 1985: Analysis of general circulation model sea-surface temperature anomaly simulations using a linear model. Part I: Forced solutions. *J. Atmos. Sci.,* **42,** 2225–2241.

Broccoli, A. J., and S. Manabe, 1992: The effects of orography on midlatitude Northern Hemisphere dry climates. *J. Climate,* **5,** 1181–1201.

Cadet, D. L., 1985: The Southern Oscillation over the Indian Ocean. *Int. J. Climatol.,* **5,** 189–212.

Cayan, D. R., 1990: Variability of latent and sensible heat flux over the oceans. Ph.D. thesis, University of California, San Diego, 199 pp.

Chambers, D. P., B. D. Tarpley, and R. H. Stewart, 1999: Anomalous warming in the Indian Ocean coincident with El Niño. *J. Geophys. Res.,* **104,** 3035–3047.

Collins, J. A., J. D. Scott, C. A. Smith, and M. A. Alexander, 2001: The GFDL Electronic Climate Atlas. [Available online at http://www.cdc.noaa.gov/gfdl.]

Covey, D. L., and S. Hastenrath, 1978: The Pacific El Niño phenomenon in the Atlantic sector. *Mon. Wea. Rev.,* **106,** 1280–1287.
Curtis, S., and S. Hastenrath, 1995: Forcing of anomalous sea surface temperature evolution in the tropical Atlantic during Pacific warm events. *J. Geophys. Res.,* **100,** 15 835–15 847.
Dayton, P. K., and M. J. Tegner, 1990: Bottoms beneath troubled waters: Benthic impacts of the 1982–1984 El Niño in the temperate zone. *Global Ecological Consequences of the 1982–83 El Niño–Southern Oscillation,* P. W. Glynn, Ed., Elsevier, 433–472.
Deser, C., and M. L. Blackmon, 1995: On the relationship between tropical and North Pacific sea surface temperature variations. *J. Climate,* **8,** 1677–1680.
——, M. A. Alexander, and M. S. Timlin, 1996: Upper-ocean thermal variations in the North Pacific during 1970–1991. *J. Climate,* **9,** 1841–1855.
Emery, W. J., and K. Hamilton, 1985: Atmospheric forcing of interannual variability in the northeast Pacific Ocean: Connections with El Niño. *J. Geophys. Res.,* **90,** 857–868.
Enfield, D. B., and D. A. Mayer, 1997: Tropical Atlantic sea surface temperature variability and its relation to El Niño–Southern Oscillation. *J. Geophys. Res.,* **102,** 929–945.
——, and A. M. Mestas-Nuñez, 1999: Multiscale variabilities in global sea surface temperatures and their relationships with tropospheric climate patterns. *J. Climate,* **12,** 2719–2733.
Ferranti, L., F. Molteni, and T. N. Palmer, 1994: Impact of localized tropical and extratropical SST anomalies in ensembles of seasonal GCM integrations. *Quart. J. Roy. Meteor. Soc.,* **120,** 1613–1645.
Frankignoul, C., 1985: Sea surface temperature anomalies, planetary waves, and air–sea feedback in the middle latitudes. *Rev. Geophys.,* **23,** 357–390.
——, and R. W. Reynolds, 1983: Testing a dynamical model for midlatitude sea surface temperature anomalies. *J. Phys. Oceanogr.,* **13,** 1131–1145.
Garreaud, R. D., and D. S. Battisti, 1999: Interannual (ENSO) and interdecadal (ENSO-like) variability in the Southern Hemisphere tropospheric circulation. *J. Climate,* **12,** 2113–2123.
Gaspar, P., 1988: Modeling the seasonal cycle of the upper ocean. *J. Phys. Oceanogr.,* **18,** 161–180.
Giannini, A., Y. Kushnir, and M. A. Cane, 2000: Interannual variability of Caribbean rainfall, ENSO, and the Atlantic Ocean. *J. Climate,* **13,** 297–311.
Gill, A. E., 1980: Some simple solutions for heat-induced tropical circulation. *Quart. J. Roy. Meteor. Soc.,* **106,** 447–462.
Gordon, C. T., and W. Stern, 1982: A description of the GFDL global spectral model. *Mon. Wea. Rev.,* **110,** 625–644.
Graham, N. E., T. P. Barnett, R. Wilde, M. Ponater, and S. Scuhbert, 1994: On the roles of tropical and midlatitude SSTs in forcing annual to interdecadal variability in the winter Northern Hemisphere circulation. *J. Climate,* **7,** 1416–1442.
Gu, D., and S. G. H. Philander, 1997: Interdecadal climate fluctuations that depend on exchanges between the tropics and extratropics. *Science,* **275,** 805–807.
Hanawa, K. T., T. Watanabe, N. Iwasaka, and T. Suga, 1988: Surface thermal conditions in the western North Pacific during the ENSO events. *J. Meteor. Soc. Japan,* **66,** 445–456.
——, Y. Yoshikawa, and T. Watanabe, 1989: Composite analyses of wintertime wind stress vector fields with respect to SST anomalies in the western North Pacific and the ENSO events. Part I: SST composite. *J. Meteor. Soc. Japan,* **67,** 385–400.
Harrison, D. E., and N. K. Larkin, 1998: El Niño–Southern Oscillation sea surface temperature and wind anomalies. *Rev. Geophys.,* **36,** 353–399.
Hastenrath, S., L. C. Castro, and P. Aceituno, 1987: The Southern Oscillation in the Atlantic sector. *Contrib. Atmos. Phys.,* **60,** 447–463.
Held, I. M., S. W. Lyons, and S. Nigam, 1989: Transients and the extratropical response to El Niño. *J. Atmos. Sci.,* **46,** 163–174.
Hendon, H. H., and D. L. Hartmann, 1982: Stationary waves on a sphere: Sensitivity to thermal feedback. *J. Atmos. Sci.,* **39,** 1906–1920.
Hoerling, M. P., and A. Kumar, 2002: Atmospheric response patterns associated with tropical forcing. *J. Climate,* **15,** 2184–2203.
Horel, J. D., and J. M. Wallace, 1981: Planetary-scale atmospheric phenomena associated with the interannual variability of sea surface temperature in the equatorial Pacific. *Mon. Wea. Rev.,* **109,** 813–829.
Hoskins, B. J., and D. J. Karoly, 1981: The steady linear response of a spherical atmosphere to thermal and orographic forcing. *J. Atmos. Sci.,* **38,** 1179–1196.
Hsiung, J., and R. E. Newell, 1983: The principal nonseasonal modes of variation of global sea surface temperature. *J. Phys. Oceanogr.,* **13,** 1957–1967.
Iwasaka, N., and J. M. Wallace, 1995: Large scale air sea interaction in the Northern Hemisphere from a view point of variations of surface heat flux by SVD analysis. *J. Meteor. Soc. Japan,* **73,** 781–794.
Jacobs, G. A., H. E. Hurlburt, J. C. Kindle, E. J. Metzger, J. L. Mitchell, and A. J. Wallcraft, 1994: Decade-scale trans-Pacific propagation and warming effects of an El Niño anomaly. *Nature,* **370,** 360–363.
Johnson, M. A., and J. J. O'Brien, 1990: The northeast Pacific Ocean response to the 1982–1983 El Niño. *J. Geophys. Res.,* **95,** 7155–7166.
Kalnay, E., and Coauthors, 1996: The NCEP/NCAR 40-Year Reanalysis Project. *Bull. Amer. Meteor. Soc.,* **77,** 437–471.
Kawamura, R., 1994: A rotated EOF analysis of global sea surface temperature variability with interannual and interdecadal scales. *J. Phys. Oceanogr.,* **24,** 707–715.
Kendall, M., and A. Stuart, 1977: *The Advanced Theory of Statistics.* 3d ed. Vol. 1, Macmillian, 283 pp.
Kiladis, G. N., and H. F. Diaz, 1989: Global climate anomalies associated with extremes in the Southern Oscillation. *J. Climate,* **2,** 1069–1090.
Kistler, R., and Coauthors, 2001: The NCEP–NCAR 50-Year Reanalysis: Monthly means CD-ROM and documentation. *Bull. Amer. Meteor. Soc.,* **82,** 247–267.
Klein, S. A., B. J. Soden, and N.-C. Lau, 1999: Remote sea surface variations during ENSO: Evidence for a tropical atmospheric bridge. *J. Climate,* **12,** 917–932.
Kok, C. J., and J. D. Opsteegh, 1985: Possible causes of anomalies in seasonal mean circulation patterns during the 1982–83 El Niño event. *J. Atmos. Sci.,* **42,** 677–694.
Kumar, A., and M. P. Hoerling, 1995: Prospects and limitations of seasonal atmospheric GCM predictions. *Bull. Amer. Meteor. Soc.,* **76,** 335–345.
——, and ——, 1998: Specification of regional sea surface temperatures in atmospheric general circulation model simulations. *J. Geophys. Res.,* **103,** 8901–8907.
Kushnir, Y., W. A. Robinson, I. Bladé, N. M. J. Hall, S. Peng, and R. Sutton, 2002: Atmospheric GCM response to extratropical SST anomalies: Synthesis and evaluation. *J. Climate,* **15,** 2233–2256.
Lanzante, J., 1996: Lag relationships involving tropical sea surface temperatures. *J. Climate,* **9,** 2568–2578.
Latif, M., 2000: Tropical Pacific/Atlantic Ocean interactions at multidecadal time scales. Max Planck Institute Rep. 305, Hamburg, Germany, 13 pp.
——, and T. P. Barnett, 1994: Causes of decadal climate variability over the North Pacific and North America. *Science,* **266,** 634–637.
——, and ——, 1995: Interactions of the tropical oceans. *J. Climate,* **8,** 952–964.
——, and ——, 1996: Decadal climate variability over the North Pacific and North America: Dynamics and predictability. *J. Climate,* **9,** 2407–2423.
——, E. Roeckner, U. Mikolajewivz, and R. Voss, 2000: Tropical stabilization of the thermohaline circulation in a greenhouse warming. *J. Climate,* **13,** 1809–1813.

Lau, N.-C., 1997: Interactions between global SST anomalies and the midlatitude atmospheric circulation. *Bull. Amer. Meteor. Soc.,* **78,** 21–33.
——, and M. J. Nath, 1994: A modeling study of the relative roles of tropical and extratropical SST anomalies in the variability of the global atmosphere–ocean system. *J. Climate,* **7,** 1184–1207.
——, and ——, 1996: The role of the ''atmospheric bridge'' in linking tropical Pacific ENSO events to extratropical SST anomalies. *J. Climate,* **9,** 2036–2057.
——, and ——, 2000: Impact of ENSO on the variability of the Asian–Australian monsoons as simulated in GCM experiments. *J. Climate,* **13,** 4287–4309.
——, and ——, 2001: Impact of ENSO on SST variability in the North Pacific and North Atlantic: Seasonal dependence and role of extratropical air–sea coupling. *J. Climate,* **14,** 2846–2866.
Lockyer, N., and W. J. S. Lockyer, 1902: On the similarity of the short-period pressure variations over large areas. *Proc. Roy. Soc. London,* **71,** 134–136.
Lukas, R., and E. Lindstrom, 1991: The mixed layer of the western equatorial Pacific Ocean. *J. Geophys. Res.,* **96,** 3343–3357.
Luksch, U., and H. von Storch, 1992: Modeling the low-frequency sea surface temperature variability in the North Pacific. *J. Climate,* **5,** 893–906.
——, ——, and E. Maier-Reimer, 1990: Modeling North Pacific SST anomalies as a response to anomalous atmospheric forcing. *J. Mar. Syst.,* **1,** 51–60.
Manabe, S., and R. J. Stouffer, 1996: Low-frequency variability of surface air temperature in a 1000-year integration of a coupled atmosphere–ocean–land surface model. *J. Climate,* **9,** 376–393.
Mantua, N. J., S. R. Hare, Y. Zhang, J. M. Wallace, and R. Francis, 1997: A Pacific interdecadal climate oscillation with impacts on salmon production. *Bull. Amer. Meteor. Soc.,* **78,** 1069–1079.
Matsuno, T., 1966: Quasi-geostrophic motions in the equatorial area. *J. Meteor. Soc. Japan,* **44,** 25–43.
Mestas-Nuñez, A. M., and D. B. Enfield, 1999: Rotated global modes of non-ENSO sea surface temperature variability. *J. Climate,* **12,** 2734–2746.
Miller, A. J., and N. Schneider, 2000: Interdecadal climate regime dynamics in the North Pacific Ocean: Theories, observations, and ecosystem impacts. *Progress in Oceanography*, Vol. 47, Pergamon, 355–379.
——, D. R. Cayan, T. P. Barnett, N. E. Graham, and J. M. Oberhuber, 1994: Interdecadal variability of the Pacific Ocean: Model response to observed heat flux and wind stress anomalies. *Climate Dyn.,* **10,** 287–302.
——, W. B. White, and D. R. Cayan, 1997: North Pacific thermocline variations on ENSO timescales. *J. Phys. Oceanogr.,* **27,** 2023–2039.
Monterey, G. I., and S. Levitus, 1997: Climatological cycle of mixed layer depth in the world ocean. NOAA/NESDIS, U.S. Govt. Printing Office, 5 pp.
Moron, V., R. Vautard, and M. Ghil, 1998: Trends, interdecadal and interannual oscillations in global sea-surface temperatures. *Climate Dyn.,* **14,** 545–569.
Murtugudde, R., and A. Busalachi, 1999: Interannual variability of the dynamics and thermodynamics of the tropical Indian Ocean. *J. Climate,* **12,** 2300–2326.
Mysak, L. A., 1986: El Niño, interannual variability and fisheries in the northeast Pacific Ocean. *Can. J. Fish. Aquat. Sci.,* **43,** 464–497.
Nakamura, H., G. Lin, and T. Yamagata, 1997: Decadal climate variability in the North Pacific in recent decades. *Bull. Amer. Meteor. Soc.,* **78,** 2215–2226.
Namias, J., 1976: Some statistical and synoptic characteristics associated with El Niño. *J. Phys. Oceanogr.,* **6,** 130–138.
——, and R. M. Born, 1970: Temporal coherence in North Pacific sea-surface temperature patterns. *J. Geophys. Res.,* **75,** 5952–5955.
——, and ——, 1974: Further studies of temporal coherence in North Pacific sea surface temperatures. *J. Geophys. Res.,* **79,** 797–798.
Newman, M., and P. D. Sardeshmukh, 1998: The impact of the annual cycle on the North Pacific/North American response to remote low-frequency forcing. *J. Atmos. Sci.,* **55,** 1336–1353.
——, M. A. Alexander, C. R. Winkler, J. D. Scott, and J. J. Barsugli, 2000: A linear diagnosis of the coupled extratropical ocean–atmosphere system in the GFDL GCM. *Atmos. Sci. Lett.,* **1,** 14–25.
Nicholson, S. E., 1997: An analysis of the ENSO signal in the tropical Atlantic and western Indian Oceans. *Int. J. Climatol.,* **17,** 345–375.
Niebauer, H. J., 1984: On the effect of El Niño events in Alaskan waters. *Bull. Amer. Meteor. Soc.,* **65,** 472–473.
——, 1988: Effects of El Niño–Southern Oscillation and North Pacific weather patterns on interannual variability in the southern Bering Sea. *J. Geophys. Res.,* **93,** 5051–5068.
Nitta, T., and S. Yamada, 1989: Recent warming of tropical sea surface temperature and its relationship to the Northern Hemisphere circulation. *J. Meteor. Soc. Japan,* **67,** 375–383.
Pan, Y. H., and A. H. Oort, 1983: Global climate variations connected with sea surface temperature anomalies in the eastern equatorial Pacific Ocean for the 1958–73 period. *Mon. Wea. Rev.,* **111,** 1244–1258.
——, and ——, 1990: Correlation analyses between sea surface temperature anomalies in the eastern equatorial Pacific and the world ocean. *Climate Dyn.,* **4,** 191–205.
Pares-Sierra, A., and J. J. O'Brien, 1989: The seasonal and interannual variability of the California Current System: A numerical model. *J. Geophys. Res.,* **94,** 3159–3180.
Peng, S., W. A. Robinson, and M. P. Hoerling, 1997: The modeled atmospheric response to midlatitude SST anomalies and its dependence on background circulation states. *J. Climate,* **10,** 971–987.
Penland, C., and P. D. Sardeshmukh, 1995: The optimal growth of tropical sea surface temperature anomalies. *J. Climate,* **8,** 1999–2024.
——, and L. Matrosova, 1998: Prediction of tropical Atlantic sea surface temperatures using linear inverse modeling. *J. Climate,* **11,** 483–496.
Pierce, D. W., T. P. Barnett, and M. Latif, 2000: Connections between the Pacific Ocean Tropics and midlatitudes on decadal timescales. *J. Climate,* **13,** 1173–1194.
Polovina, J. J., G. T. Mitchum, and G. T. Evans, 1995: Decadal and basin-scale variation in mixed layer depth and the impact on biological production in the central and North Pacific, 1960–88. *Deep-Sea Res.,* **42,** 1701–1716.
Qiu, B., 2000: Interannual variability of the Kuroshio extension system and its impact on the wintertime SST field. *J. Phys. Oceanogr.,* **30,** 1486–1502.
Rasmusson, E. M., and T. H. Carpenter, 1982: Variations in tropical sea surface temperature and surface wind fields associated with the Southern Oscillation/El Niño. *Mon. Wea. Rev.,* **110,** 354–384.
Reynolds, R. W., and E. M. Rasmusson, 1983: The North Pacific sea surface temperature associated with El Niño events. *Proc. Seventh Annual Climate Diagnostics Workshop,* Boulder, CO, NOAA/NCEP/CPC, 298–310. [NTIS PB283-208033.]
——, and T. M. Smith, 1994: Improved global sea surface temperature analyses using optimum interpolation. *J. Climate,* **7,** 929–948.
Rienecker, M. M., and C. N. K. Mooers, 1986: The 1982–1983 El Niño signal off northern California. *J. Geophys. Res.,* **91,** 6597–6608.
Robinson, W. A., 2000: Review of WETS—The Workshop on Extra-Tropical SST Anomalies. *Bull. Amer. Meteor. Soc.,* **81,** 567–577.
Rodwell, M. J., D. P. Rowell, and C. K. Folland, 1999: Oceanic forcing of the wintertime North Atlantic Oscillation and European climate. *Nature,* **398,** 320–323.
Ropelewski, C. F., and M. S. Halpert, 1987: Global and regional scale precipitation patterns associated with the El Niño/Southern Oscillation. *Mon. Wea. Rev.,* **115,** 1606–1626.
Rowntree, P. R., 1972: The influence of tropical east Pacific Ocean

temperatures on the atmosphere. *Quart. J. Roy. Meteor. Soc.*, **98,** 290–321.
Saji, N. H., B. N. Goswami, P. N. Vinayachandran, and T. Yamagata, 1999: A dipole mode in the tropical Indian Ocean. *Nature,* **401,** 360–363.
Saravanan, R., 1998: Atmospheric low frequency variability and its relationship to midlatitude SST variability: Studies using the NCAR Climate System Model. *J. Climate,* **11,** 1386–1404.
——, and P. Chang, 2000: Interaction between tropical Atlantic variability and El Niño–Southern Oscillation. *J. Climate,* **13,** 2177–2194.
Sardeshmukh, P. D., and B. J. Hoskins, 1988: The generation of global rotational flow by steady, idealized tropical divergence. *J. Atmos. Sci.,* **45,** 1228–1251.
——, G. P. Compo, and C. Penland, 2000: Changes of probability associated with El Niño. *J. Climate,* **13,** 4268–4286.
Schmittner, A., C. Appenzeller, and T. F. Stocker, 2000: Enhanced Atlantic freshwater export during El Niño. *Geophys. Res. Lett.*, **27,** 1163–1666.
Scott, J. D., and M. A. Alexander, 1999: Net shortwave fluxes over the ocean. *J. Phys. Oceanogr.,* **29,** 3167–3174.
Simmons, A. J., J. M. Wallace, and G. W. Branstator, 1983: Barotropic wave propagation and instability, and atmospheric teleconnection patterns. *J. Atmos. Sci.,* **40,** 1363–1392.
Simpson, J. J., 1983: Large scale thermal anomalies in the California current during the 1982–83 El Niño. *Geophys. Res. Lett.,* **10,** 937–940.
Smith, T. M., R. W. Reynolds, R. E. Livezey, and D. C. Stokes, 1996: Reconstruction of historical sea surface temperatures using empirical orthogonal functions. *J. Climate,* **9,** 1403–1420.
Ting, M., and P. D. Sardeshmukh, 1993: Factors determining the extratropical response to equatorial diabatic heating anomalies. *J. Atmos. Sci.,* **50,** 907–918.
——, and S. Peng, 1995: Dynamics of early and midwinter responses to the northwest Atlantic SST anomalies. *J. Climate,* **8,** 2239–2254.
Tourre, Y. M., and W. B. White, 1995: ENSO signals in global upper-ocean temperature. *J. Phys. Oceanogr.,* **25,** 1317–1332.
Trenberth, K. E., 1997: The definition of El Niño. *Bull. Amer. Meteor. Soc.,* **78,** 2771–2778.
——, and J. D. A. Paolino, 1981: Characteristic patterns of variability of sea level pressure in the Northern Hemisphere. *Mon. Wea. Rev.,* **109,** 1169–1189.
——, and J. W. Hurrell, 1994: Decadal atmosphere–ocean variations in the Pacific. *Climate Dyn.,* **9,** 303–319.
——, G. W. Branstator, D. Karoly, A. Kumar, N.-C. Lau, and C. Ropelewski, 1998: Progress during TOGA in understanding and modeling global teleconnections associated with tropical sea surface temperatures. *J. Geophys. Res.,* **103,** 14 291–14 324.
Uvo, C. B., C. A. Repelli, S. E. Zebiak, and Y. Kushnir, 1998: The relationships between tropical Pacific and Atlantic SST and northeast Brazil monthly precipitation. *J. Climate,* **11,** 551–561.
van Loon, H., and R. A. Madden, 1981: The Southern Oscillation. Part I. Global associations with pressure and temperature in northern winter. *Mon. Wea. Rev.,* **109,** 1150–1162.
Venzke, S., M. Latif, and A. Villwock, 2000: The coupled GCM ECHO-2. Part II: Indian Ocean response to ENSO. *J. Climate,* **13,** 1384–1405.
Vimont, D. J., D. S. Battisti, and A. C. Hirst, 2001: Footprinting: A seasonal connection between the tropics and mid-latitudes. *Geophys. Res. Lett.,* **28,** 3923–3926.
Wagner, A. J., 1984: Possible mid-latitude atmospheric generation of anomalously warm surface waters in the Gulf of Alaska from autumn 1982 to spring 1983. *Tropical Ocean–Atmosphere Newsletter,* No. **26,** 15–16.
Walker, G. T., 1909: Correlation in seasonal variation of climate. *Mem. India Meteor. Dept.,* **20,** 117–124.
——, 1924: Correlation in seasonal variations of weather IX. *Mem. India Meteor. Dept.,* **24,** 275–332.
——, and E. W. Bliss, 1932: World Weather V. *Mem. Roy. Meteor. Soc.,* **4,** 53–84.
Wallace, J. M., and Q. Jiang, 1987: On the observed structure of the interannual variability of the atmosphere/ocean climate system. *Atmospheric and Oceanic Variability,* H. Cattle, Ed., Royal Meteorological Society, 17–43.
——, E. M. Rasmusson, T. P. Mitchell, V. E. Kousky, E. S. Sarachik, and H. von Storch, 1998: On the structure and evolution of ENSO-related climate variability in the tropical Pacific: Lessons from TOGA. *J. Geophys. Res.,* **103,** 14 241–14 260.
Wang, B., R. Wu, and X. Fu, 2000: Pacific–East Asian teleconnection: How does ENSO affect east Asian climate. *J. Climate,* **13,** 1517–1536.
Wang, H., and R. Fu, 2000: Winter monthly mean atmospheric anomalies over the North Pacific and North America associated with El Niño SSTs. *J. Climate,* **13,** 3435–3447.
Watanabe, M., and M. Kimoto, 2000: On the persistence of decadal SST anomalies in the North Atlantic. *J. Climate,* **13,** 3017–3028.
Weare, B. C., A. R. Navato, and R. E. Newell, 1976: Empirical orthogonal analysis of Pacific Ocean sea surface temperatures. *J. Phys. Oceanogr.,* **6,** 671–678.
Webster, P. J., A. M. Moore, J. P. Loschnig, and R. R. Leben, 1999: Coupled ocean–atmosphere dynamics in the Indian Ocean during 1997–98. *Nature,* **401,** 356–360.
White, W. B., 1995: Design of a global observing system for gyre-scale upper ocean temperature variability. *Progress in Oceanography,* Vol. 36, Pergamon, 169–217.
Wilks, D. S., 1995: *Statistical Methods in the Atmospheric Sciences.* Academic Press, 467 pp.
Winkler, C. R., M. Newman, and P. D. Sardeshmukh, 2001: A linear model of wintertime low-frequency variability. Part I: Formulation and forecast skill. *J. Climate,* **14,** 4474–4494.
Wolter, K., 1987: The Southern Oscillation in surface circulation and climate over the tropical Atlantic, eastern Pacific, and Indian Oceans as captured by cluster analysis. *J. Climate Appl. Meteor.,* **26,** 540–541.
——, 1989: Modes of tropical circulation, Southern Oscillation, and Sahel rainfall anomalies. *J. Climate,* **2,** 149–172.
Wright, P. B., 1983: Sea surface temperature fluctuations in the Pacific, 0°–50°N. *Tropical Ocean–Atmosphere Newsletter,* No. 19, 14–15.
Xie, P., and P. A. Arkin, 1997: Global precipitation: A 17-year monthly analysis based on gauge observations, satellite estimates, and numerical model outputs. *Bull. Amer. Meteor. Soc.,* **78,** 2539–2558.
Yasunari, T., 1987: Global structure of the El Niño/Southern Oscillation. Part I. El Niño composites. *J. Meteor. Soc. Japan,* **65,** 67–79.
Yu, L., and M. M. Rienecker, 1999: Mechanisms for the Indian Ocean warming during the 1997–1998 El Niño. *Geophys. Res. Lett.,* **26,** 735–738.
Yulaeva, E., N. Schneider, D. W. Pierce, and T. P. Barnett, 2001: Modeling of North Pacific climate variability forced by oceanic heat flux anomalies. *J. Climate,* **14,** 4027–4046.
Zhang, X., J. Sheng, and A. Shabbar, 1998: Modes of interannual and interdecadal variability of Pacific SST. *J. Climate,* **11,** 2556–2569.
Zhang, Y., and J. M. Wallace, 1996: Is climate variability over the North Pacific a linear response to ENSO? *J. Climate,* **9,** 1468–1478.
——, ——, and D. S. Battisti, 1997: ENSO-like interdecadal variability. *J. Climate,* **10,** 1004–1020.
Zhao, Y. P., and G. A. McBean, 1986: Annual and interannual variability of the North Pacific ocean–atmosphere total heat transfer. *Atmos.–Ocean,* **24,** 283–291.